UNIVERSITY OF GHANA

COLLEGE OF BASIC AND APPLIED SCIENCES

EVALUATION OF SURFACE DOSES AND EFFECT OF AIR GAPS UNDER BOLUS DURING EXTERNAL PHOTON BEAM RADIOTHERAPY

BY

LAMPTEY PAPA NII ODARTEY

(10599782)

THIS THESIS IS SUBMITTED TO THE UNIVERSITY OF GHANA, LEGON IN PARTIAL FULFILMENT OF THE REQUIREMENT FOR THE AWARD OF MPHIL MEDICAL PHYSICS DEGREE

JULY, 2018

DECLARATION

This thesis is the result of research work undertaken by Papa Nii Odartey Lamptey in the Department of Medical Physics, School of Nuclear and Allied Sciences, University of Ghana, under the supervision of Prof. Cyril Schandorf, Mr. George Felix Acquah and Dr. Edem Sosu.

I hereby affirm that the work done in this thesis is as a result of my own research and that no part of it has been presented for the award of any other degree in this University or elsewhere. All other works and/or researches done by other researchers cited in this work have been duly acknowledged under references.

……	……
PAPA NII ODARTEY LAMPTEY	PROF. CYRIL SCHANDORF
(STUDENT)	(PRINCIPAL SUPERVISOR)
Date…….	Date…….
……	……
MR. GEORGE FELIX ACQUAH	DR. EDEM SOSU
(CO-SUPERVISOR)	(CO-SUPERVISOR)
Date…….	Date…….

ABSTRACT

This study was performed to evaluate surface doses and the effect of air gaps under bolus on surface dose during external beam radiotherapy for photon beam energies of 6 MV and 15 MV. Surface doses were measured by using calibrated GafChromic EBT3 films and the Roos chamber for various bolus-to-surface distances (including no bolus and bolus placed directly on the RW3 phantom surface) and various field sizes. Dose verification was also done for beam energies of 6 MV and 15 MV on the RANDO phantom by measuring doses at d_{max} using a diode. The introduction of the bolus increased the surface dose for all field sizes and beam energies. For 5×5 cm^2 the surface dose increased by 61% and 72% with the introduction of the bolus for 6 MV and 15 MV respectively using the Roos chamber. For both 6 MV and 15 MV, surface doses increased significantly with the introduction of the bolus. Also, due to more skin sparing in 15 MV than 6 MV, surface doses recorded for the 6 MV photons were generally of higher value than those for the 15 MV photons especially for field sizes that were smaller. As the bolus-to-surface distance increased, the doses recorded at the surface decreased. This decrease however was seen for the small field sizes (5×5 cm^2 and 10×10 cm^2). For field sizes that were larger (15×15 cm^2 and 20×20 cm^2) the change in dose to the surface as a result of change in air gap was negligible. For 5×5 cm^2, dose to the surface decreased by 21% and 33% with a 5 cm air gap for 6 MV and 15 MV respectively compared to 20×20 cm^2 field, where the change was negligible with only a 2% and 1% increase in surface dose recorded for both 6 MV and 15 MV respectively when the ion chamber was used. The field size of 5×5 cm^2 showed the most variation of surface dose with changing air

gaps showing that change in skin dose as a result of air gaps is only significant for small field sizes.

DEDICATION

This work is dedicated to the Lord God Almighty for the wisdom, strength, grace and love He has given me throughout all these years of my academic pursuits. I also dedicate this work to Mr. Stanley Lamptey and Mrs. Olivia Lamptey, my wonderful parents for the encouragement and financial aid they have given me throughout my study.

ACKNOWLEDGEMENTS

My overwhelming gratitude to the Lord God Almighty whose grace, mercy and favor has allowed me finish this work with success.

I am also especially grateful for the aid my supervisors; Prof. Cyril Schandorf, Mr. George Felix Acquah and Dr. Edem Sosu have given me throughout this study. Indeed without their assistance this work would not have been completed. I will never forget the patience, tolerance, guidance and support they gave me whilst I undertook this study. God richly bless them for their efforts.

My appreciations also go all staff of the Oncology Department at Sweden Ghana Medical Centre and the staff of the Medical Physics Department at Korle-Bu Teaching Hospital in guiding and assisting me obtain data for my study by allowing me access to the equipment and materials in their respective departments.

I am also grateful to my Head of Department, Dr. Francis Hasford, for his sound words of advice and support as I undertook this study.

Last and not least, to my lecturers and fellow students, I say a big thank. May God bless you for your company and your willingness to help whenever I have needed it.

TABLE OF CONTENTS

LIST OF FIGURES

LIST OF PLATES

LIST OF TABLES

LIST OF ABBREVIATIONS

IAEA	International Atomic Energy Agency
SGMC	Sweden Ghana Medical Centre
MPHIL	Master of Philosophy
ICRU	International Commission on Radiation Units and Measurements
CT	Computed Tomography
MU	Monitor Units
IGRT	Image Guided Radiation Therapy
MV	Mega Voltage
TPS	Treatment Planning System
CPE	Charged Particle Equilibrium
LINAC	Linear Accelerator
d_{max}	Depth of Maximum Dose
MLC	Multileaf Collimator
PDD	Percentage Depth Dose
ICRP	International Commission on Radiological Protection
Co-60	Cobalt-60 Teletherapy Unit
VMAT	Volumetric-Modulated Arc Therapy
^{60}CO	Cobalt-60 Teletherapy Unit
D_{max}	Maximum Dose
SSD	Source-to-Surface Distance
IMRT	Intensity Modulated Radiation Therapy
RGB	Red Green Blue
TG	Task Group
EBRT	External Beam Radiation Therapy

D_{surf}	Surface Dose
RF	Radio Frequency
TLD	Thermo Luminescence Detectors
ID	Identification
ROI	Region of Interest
TRS	Technical Report Series
2-D	Two dimensional

CHAPTER ONE

INTRODUCTION

1.1 Background

Radiotherapy is a form of therapy that involves using ionizing radiation to destroy or limit the spread of malignant cells and is used in the treatment of cancer (Baskar et al., 2012). Radiation doses can be administered to a patient either by targeting the tumour using an external beam (teletherapy) or by placing the source of radiation close to the tumour (brachytherapy) (Fuller & Thomas, 2008). During teletherapy, photon beams of high energy are directed to target tumours situated deep in the patient's body whereas electron beams are used for targeting tumours in close proximity to the skin as seen in the treatment of skin cancer. External beam radiotherapy in most modern medical facilities is normally administered using a Linear Accelerator (LINAC). The intent for radiotherapy treatment can be divided into two; curative and palliative purposes. Curative radiotherapy is administered to kill malignant cells so as to cure the disease. However palliative radiotherapy is administered to reduce the rate of growth of the tumour and relieve pain because the tumour has developed to a stage where treatment can no longer be effective (Ettinger & Feldman, 2009).

The goal in any radiotherapy procedure is to administer maximum dose to the malignant cells whereas normal tissues receive minimum dose (Walsh & Crumbie, 2007). ICRU Report 62 recommends that the target volume be encompassed within the area that receives at least 95% of the prescribed dose when radiotherapy is administered (ICRU, 1999). Nonetheless, a substantial amount of dose may not be deposited on the skin

surface as a result of the skin sparing effect that occurs with megavoltage beams (radiation beams of high energy) which is attributed to the dose build-up between the regions of the skin surface and point where the maximum dose is deposited (Hillier et al., 1996). The skin sparing effect depends highly on beam specifications like field size, source-to-surface distance (SSD), beam energy and use of beam modifying devices. High energy photon beams in most cases deposit low dose to the skin surface (D_{Surf}) and estimations reveal that D_{Surf} can be as low as 25% of the dose measured at d_{max}. In treating tumours on the skin or in close proximity to surface of the skin, bolus is positioned on the skin surface so that the dose deposited at the surface of the skin increases. The dose build-up effect is recognised most in photon beams in the megavoltage range (Khan & Gibbons, 2014; Khan et al., 2013).

In radiotherapy, a bolus refers to a flexible tissue equivalent material that is employed when treating uneven areas of a patient to make up for missing tissue so that a flat surface is presented normal to the incident beam, or to contribute to the build-up of dose to the skin surface. The elevation in skin dose that the bolus provides is useful in alleviating the risk of near surface recurrence of tumours that is treated using megavoltage beams (Easson & Pointon, 2012). A particular thickness of bolus can be applied on the skin to change the dose administered both on the skin surface and at depth in the tissue.

Under certain conditions, because of the flexible material used in manufacturing the bolus, minute air gaps with sizes no bigger than a few millimeters may be encountered in particular portions of the field during treatment procedures (Butson et al., 2000). Even of more pressing concern is that the depth associated with the air gap present cannot be predicted and therefore it cannot be taken into consideration during treatment planning.

This can lead to the planned dose being different from the delivered dose (Kim et al., 2014). Accurate assessments of doses delivered close to the skin surface and to the skin itself in radiotherapy can contribute essential information to be factored clinically to alleviate recurrence near the surface while also limit extreme skin toxicity at the same time (Hsu et al., 2008). The study seeks to perform surface dose measurements to evaluate the effect that air gaps introduced by bolus have on skin surface and determine whether these air gaps have severe impact on the dose delivered to the skin during external beam radiotherapy.

1.2 Problem statement

The application of bolus in radiotherapy is used to compensate for irregular patient body contours and tissue heterogeneities so that uniform dose distribution can be achieved which complies with ICRU report 50, (1993) which requires that a uniform dose distribution within +7% and -5% of the dose prescription be achieved (Jones, 1994). Also the recommendations made by the ICRU require that the error related to the accuracy in administering absorbed dose be within ±5% (ICRU, 1976). The existence of air gaps under the bolus can alter the dose received by the skin surface and consequently the total dose deposited at d_{max}. This can ultimately lead to inadequate treatment of the tumour and increases the probability of reoccurrence. It is therefore imperative that we take into consideration the effects of the existence of these air gaps under the bolus during radiotherapy because of its possible biological implications. This study seeks to investigate the degree to which the air gaps alter administered doses.

1.3 Objective of the study

The main objective of this study is to evaluate the implications of air gaps under bolus on surface doses during external photon beam radiotherapy. The specific objectives are:

1. To determine the surface dose when varying air gaps are introduced for different field sizes and beam energies.
2. To verify doses using an anthropomorphic phantom.
3. To make appropriate recommendations from the findings.

1.4 Relevance and Justification

Due to the fact that mega voltage photon beams cause skin sparing at the surface of the skin, doses measured at the surface of the skin are usually lower than prescribed doses. The bolus is therefore positioned on the skin's surface to act as a supplementary tissue to increase the skin surface dose. However the introduction of air gaps due to the improper disposition or shift of the bolus on the skin surface can compromise the intended dose to be delivered to the skin's surface because the depth associated with the air gap cannot be predicted and therefore be taken into consideration during treatment planning. This can potentially lead to a variation when comparing the dose prescribed in planning to the actual dose delivered and can result in tumour reoccurrences or alternatively dose toxicity, both of which are detrimental to the health of the patient. It is therefore imperative to understand how air gaps under the bolus affect the prescribed dose to skin during radiation therapy. This will aid the medical physicist take into account the effects and hence make appropriate corrections to facilitate the effective delivery of the dose prescribed to the skin.

1.5 Scope and limitation

The scope of this research is in the area of external beam radiotherapy, and particularly in the implications of air gaps under bolus on surface dose. The study considers skin doses for field sizes ranging from 5×5 cm^2 to 20×20 cm^2. This study was undertaken at Sweden Ghana Medical Centre (SGMC) using the ELEKTA Linear Accelerator (LINAC). The study is phantom based.

1.6 Organization of thesis

This thesis is in a chronological order of five chapters. Chapter one presents an Introduction to the research which entails the background of the study, problem statement, objectives, relevance and justification as well as the scope and limitation. Chapter two offers a review of existing literature that is relevant to the research problem. Chapter three focuses on the materials and the methods used for the study. Chapter four is on presentation and discussion of the results obtained. The conclusion of the study, recommendations and suggestions for further research are presented in Chapter five.

CHAPTER TWO

LITERATURE REVIEW

2.1 Introduction

During external beam radiotherapy, radiation effects such as erythema, skin peeling and necrosis are liable to affect the skin. Epidemiological studies, as well, have discovered a relationship between radiotherapy and basal cell carcinoma (Kry et al., 2012). However, complications arise in skin dose due to the varying skin layers with various depths of thickness and these changes as a result of variations between patients and positions on a particular patient. ICRP recommends obtaining dose to the skin at a depth of 0.07 mm for the basal layer which is assumed to be the surface dose, whilst at 1.0 mm the dermal layer can be measured (ICRU, 1985; ICRP, 2007). Although treatment planning systems can deduce dose to the skin generally within ± 25% accuracy, CT images and a calculated treatment plan are still required (Nilsson & Brahme, 1986). A method to determine skin dose as a function of parameters for treatment was proposed by Lamb and Blake (Lamb & Blake, 1998).

2.2 Interaction of Radiation with Matter

There are three possibilities that exist when photons pass through matter. They can penetrate without interacting, be absorbed entirely by depositing all of their energy or be scattered by depositing part of their energy.

The total absorption of a photon by a core electron which causes it to be ejected from the atom is known as Photoelectric Effect. Part of the photon energy is deployed in

overcoming the binding energy of the electron and the remnant of energy is given to the electron as kinetic energy. The electron rapidly loses its energy as it moves through the surrounding matter and moves only a relatively short distance from its original location before losing all of its energy. The void the atomic shell is then occupied by an electron that drops from a greater energy state. This drop in energy produces a characteristic X-ray photon. The ejected electron is also known as a Photoelectron (Khan & Gibbons, 2014; Podgorsak, 2005).

The interaction of photons with matter where only part of the photon energy is absorbed and the photon is emitted with a lower energy than before at an angle is known as the Compton Effect (Compton Scattering). The photon moves away from the location of the interaction in a different direction from the incident photon. The original photon interacts with an electron of low binding energy (usually a valence electron) and hence a portion of the photon energy is used to eject the electron causing the scattering of the photon with a lower energy at an angle to the primary photon. However when the electron reradiates the energy of the photon at a frequency that is the same as the original photon, it is known as Coherent Scattering (other names include Rayleigh scattering and classical scattering). In this interaction, the medium does not absorb any energy and the only effect is photon scattering at angles that are minuscule. This interaction type is viable at low energies and interest shown in radiotherapy is purely academic (Khan & Gibbons, 2014; Podgorsak, 2005).

Another interaction of photons with matter is pair production where photons in excess of 1.02 MeV interact with the nucleus of an atom resulting in the conversion of the photon's energy into matter. The interaction produces an electron and a positron, both with the

same energy. A base energy of 1.02 MeV is necessary to generate the electron pair due to the electron rest mass energy being equivalent to 0.51 MeV. The positron loses it energy as it traverses the matter and when it gets close to the limit of its range, it collides with a free electron to generate two annihilation photons, with each photon having an energy of 0.51 MeV and ejected in directions opposite to each other (Khan & Gibbons, 2014; Podgorsak, 2005).

Whereas photons have interactions with matter through Compton, photoelectric, or pair production processes, charged particles (α-particles, protons, electrons, and nuclei) interact primarily by excitation and ionization. Charged particle interactions or collisions occur as a result of the Coulomb interactions between electric fields of electrons in orbit and the atomic nucleus of the material with the electric field of the traversing particle. Collisions between the atomic electrons and the particle result in atoms becoming ionized or excited whereas collisions between the nucleus and the particle result in bremsstrahlung or radiative loss of energy. Particles can also undergo scattering without a sizeable loss of energy with electrons undergoing more scattering interactions than heavier particles due to their much smaller mass (Khan & Gibbons, 2014).

2.3 Skin and build-up region doses

In treating a patient with a megavoltage beam, the skin or surface dose may be considerably lower than the maximum dose that is deposited in the subcutaneous tissues. Conversely, lower energy beams contribute to maximum ionization close to or at the skin surface (Khan & Gibbons, 2014). Megavoltage beams generate an initial electronic build-

up with depth which leads to a decrease in the dose delivered to the surface and a deposition of maximum dose at the equilibrium depth. The region of dose deposition between the surface (d = 0.0 cm) and depth d = d_{max} in megavoltage beams is termed the dose build-up region which is derived from the relatively long range of energetic secondary charged particles (β- and β+) which initially due to photon interactions are released in the patient and finally release their kinetic energy in the patient. Right underneath the surface, the condition of charged particle equilibrium (CPE) ceases to be in existence and the dose absorbed smaller than the collision kerma by a significant amount. However as the depth increases, the charged particle equilibrium gradually reaches to where d = d_{max}, where d is approximately equal to the range of secondary charged particles and therefore, comparisons can be made between collision kerma and dose. Beyond d_{max} both collision kerma and dose reduce as a result of the photon attenuation that occurs patient which leads to a transient instead of true CPE (Podgorsak, 2005).

Low surface or skin dose when compared to the maximum dose is termed skin sparing and because of this, megavoltage beams are preferred to superficial and orthovoltage beams when treating deep seated tumors. Superficial and orthovoltage beams do not show skin sparing due to the fact that the surface receives the maximum dose. Skin sparing is one of the most desired traits of high energy photon beams. Nevertheless, skin sparing may be minimized or become insignificant due to excessive electron contamination (Khan & Gibbons, 2014).

2.3.1 Electron contamination of photon beams

Surface dose arise due to the incident beam being contaminated with electrons and also from the backscattered radiation generated from that medium. It is an established fact that X-ray and gamma ray beams employed in radiotherapy are tainted with secondary electrons. The bulk of these electrons are Compton electrons that are formed by the interactions of the photon with the collimator, air, and any other material that is positioned in the beam's path that has the ability to scatter photons (Khan & Gibbons, 2014). Figure 2.1 shows the relationship between absorbed dose (D) and the collision part of kerma (K^{col}) when a photon broad beam penetrates a medium. Whereas at the surface kerma is greatest and reduces with depth, the dose first of all builds up to a maximum value and then reduces at a rate that is the same as kerma.

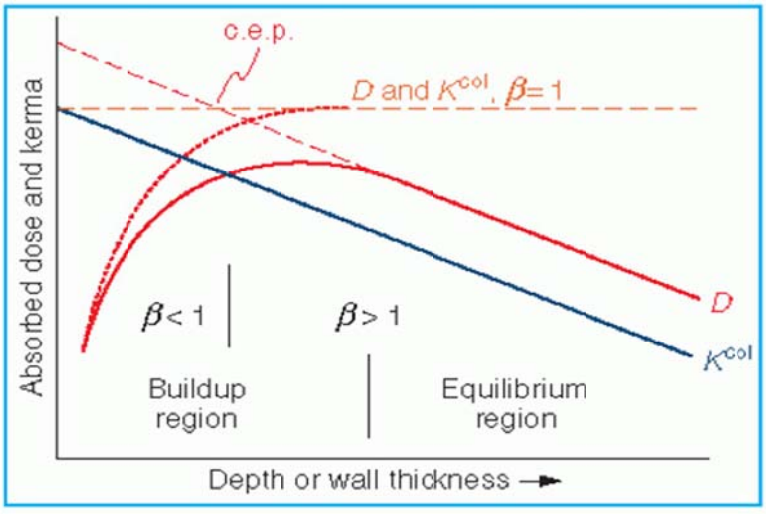

Figure 2.1: Relationship between absorbed dose D and collision kerma K^{col} for a megavoltage photon beam (Khan & Gibbons, 2014, pp. 98).

Electron contamination has an effect on the variation of dose in the build-up region as the field size changes. Depth dose in the build-up region increases with as the field size also

increases with ultimately leads to a shift in d_{max} to increasingly shallower depths (Almond et al., 1970; Johns & Rawlinson, 1976; Marinello & Dutreix, 1973). Numerous studies undertaken by researchers have revealed that this effect is predominantly caused by secondary electrons (Biggs & Ling, 1979; Marbach & Almond, 1977; Padikal & Deye, 1978).

2.3.2 Relationship between skin sparing and photon energy

Studies undertaken have indicated that distribution of dose on the skin depend on many parameters such as beam energy, field size, source-to-skin distance (SSD) and configuration of secondary blocking tray (Gerbi & Khan, 1990; Khan & Gibbons, 2014). A number of studies have discovered that at higher megavoltage energies, skin dose reduces (Kry et al., 2012; Stathakis et al., 2006) while others have not, particularly for field sizes that are larger as shown with both lower energies (6 – 10 MV) and higher energies (15 – 18 MV). Table 2.1 shows values for various energies which are provided to be exemplary and not universally accepted for all treatment machines particularly involving depths smaller than 2 mm. For greater depths, however, reasonable agreements amongst various treatment machines have been proven to exist for greater depths (Khan & Gibbons, 2014).

Table 2.1: Distribution of dose build-up in Polystyrene (10×10 cm^2).

Depth (mm)	^{60}Co 80 cm [a]	4 MV 80cm [a]	10 MV 100 cm [b]	25 MV 100 cm [a]
0	18.0	14.0	12.0	17.0
1	70.5	57.0	30.0	28.0
2	90.0	74.0	46.0	39.5
3	98.0	84.0	55.0	47.0
4	100.0	90.0	63.0	54.5
5	100.0	94.0	72.0	60.5
6	-	96.5	76.0	66.0
8	-	99.5	84.0	73.0
10	-	100.0	91.0	79.0
15	-	-	97.0	88.5
20	-	-	98.0	95.0
25	-	-	100.0	99.0
30	-	-	-	100

[a] Data obtained from Velkley, Manson, Purdy, & Oliver, (1975).

[b] Data obtained from F. M. Khan, Moore, & Levitt, (1973).

Generally, more pronounced skin sparing can be realized with high energy beams for the skin surface and subcutaneous tissues. Also, in reference to Podgorsak (2005), it has been noticed that the surface dose is lower when the photon beam energy is higher and this surface dose which typically amounts to 30% of the d_{max} dose for a ^{60}Co gamma ray beam, 15% of the d_{max} dose for a 6 MV X-ray beam and 10% of the d_{max} dose for an 18

MV X-ray beam for a 10×10 cm^2 field (Podgorsak, 2005). Butson et al. also measured skin doses and discovered them to be 22% for 6 MV photons, 17% for 10 MV photons and 15.5% for 18 MV photons (Butson et al., 1998). These measurements were taken on the central axis of the beam relative to d_{max} for a 10×10 field.

2.3.3 Depth of maximum dose d_{max}

The depth of maximum dose d_{max} below the surface of the patient relies on the field size of the beam and the energy of the beam. However, field size reliance is regularly omitted because it represents a minor effect as compared to the beam energy dependence. For specified beam energy, the largest d_{max} occurs for 5×5 cm^2 fields. For fields greater than this, d_{max} decreases as a result of collimator scatter effects in Co-60 units and collimator as well as flattening filter scatters effects in linear accelerators. Field sizes lesser than 5×5 cm^2 experience a decrease in d_{max} due to phantom scatter effects (Podgorsak, 2005).

Table 2.2 shows the nominal values for d_{max} that range from 0 to 5 cm for varying photon beam energies.

Table 2.2: d_{max} values for different photon beam energies (5×5 cm^2).

	Superficial	Orthovoltage	Co-60	4 MV	6 MV	10 MV	18 MV	25 MV
d_{max} (cm)	0	0	0.5	1	1.5	2.5	3.5	5

Data obtained from E B Podgorsak (2005).

2.3.4 Effect of field size on surface dose

Yadav et al. undertook skin dose estimations for varying beam modifiers at different SSDs for a 6 MV photon beam where an acrylic slab phantom and a Markus parallel plate ionization chamber were used to take measurements of doses deposited at the surface and doses deposited in the build-up region. Measurements were taken for open fields, motorized wedge fields, as well as for acrylic block tray fields ranging from 3 × 3 cm^2 to 30 × 30 cm^2. Their work demonstrated the increase of the size of the field with skin dose for all the beam modifiers. A conclusion was made on the block tray showing that electrons were eliminated from the upstream but generated its own new secondary electrons. The number of electrons eliminated downstream were exceeded by the electrons produced upstream hence there was an increase in skin dose. They discovered that for the 60° motorized wedge fields, the skin dose increased with field size but were lower than that for open fields. Physical wedge generated electron by itself whilst eliminating electrons from upstream (Kry et al., 2012; Yadav et al., 2009).

Increase in dose to the skin as the field size is increased generally is attributed to increased electron release from air and the collimator (Khan & Gibbons, 2014). Figure 2.2 illustrates the relationship between percentage surface dose and field size for ^{60}Co, 4 MV and 10 MV photons. The data set shows that skin sparing is substantially minimized for bigger field sizes.

Saylor & Quillin have made discussions on the relative importance of the distance between the tray and the surface of the skin and field size for ^{60}Co gamma rays. They have demonstrated that the ideal skin sparing takes place for the ratio of $\frac{h}{r}$ of about 4, where h is the tray-to-skin surface distance and r is the radius of an equivalent circular

field (Saylor & Quillin, 1971). This ratio can easily be realized for smaller fields like 5×5 cm^2 because it demands a distance of 12 cm whilst for larger fields like 30×30 cm^2, the corresponding absorber-to-surface distance is 67 cm, which is next to impossible for isocentric treatments.

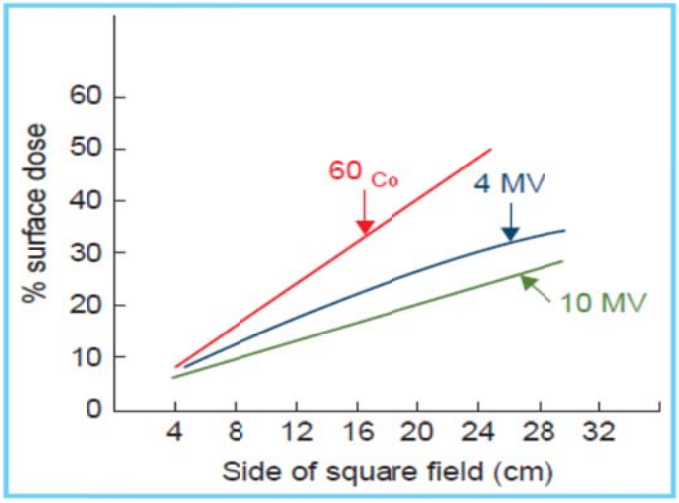

Figure 2.2: Relationship between percentage surface dose and field size (F. M. Khan & Gibbons, 2014, pp. 243).

2.4 Bolus and its effect on surface dose

A bolus is a material that is naturally or synthetically developed to act as a tissue layer to allow for a more effective treatment of superficial lesions, to correct for surface contours that vary and to add scattering material around the surface of the patient (Bentel, 1995; Khan & Gibbons, 2014). There are various types of tissue-equivalent bolus materials, some of which include; water, wet cotton gauze, uncooked rice, paraffin wax, Aquaplast, Play-Doh, Superflab, Super Stuff, Elasto-Gel, BeesWax among others (Vyas et al., 2013).

Surface dose magnitude is reliant on the use of beam modifiers, air gap, field size and the angle of the incident beam (Biggs & Ling, 1979; Gerbi & Khan, 1990; Lamb & Blake, 1998; Medina et al., 2005; Zhu & Palta, 1998). Intensity Modulated Radiotherapy (IMRT) has been proven popular when delivering megavoltage beam for surface dose measurements. Lee et al. discovered that as a result of "bolus effect" of thermoplastic shell, there was an average increase of dose deposited at the surface of about 18%. They also determined that for parallel opposed and 1MRT treatments that the doss to the surface was 84% and 100% of the prescribed dose respectively when the thermoplastic shell was applied (Lee et al., 2002).

Hsu et al. assessed skin doses for chest wall radiotherapy by quantifying changes to the doses at the surface as a function of the bolus material for both conventional and 1MRT tangential fields. They compared Superflab with other types of bolus materials specifically 2 mm solid Aquaplast, 2mm fine mesh Aquaplast and 3.2 large mesh Aquaplast. Results indicated that the difference in the surface dose was not significant when conventional radiotherapy tangential techniques was compared to IMRT tangential techniques and surface dose measured without bolus was of a much lesser value than with bolus. They also investigated that for chest wall tangential radiotherapy, the bolus effect was large with an increment of up to 82% when the 2 mm fine mesh Aquaplast was employed (Hsu et al., 2008).

Khan et al. (2003) performed a study on the effect of air gaps between the bolus and skin for 1 cm Superflab bolus on dose at the surface and at depth of dose maximum using water an anthropomorphic phantom. Measurements were taken for varying field sizes using a farmer chamber and GafChromic EBT2 films. They found out that for 5×5 cm^2

field sizes, air gaps greater than 5 mm caused a significant change in the surface dose. However for field sizes that were larger than 10×10 cm^2, there was negligible change in the surface dose measured for air gaps of 0 to 5 cm (Khan et al., 2013).

Butson et al. discovered that an air gap of 2 mm did not decrease dose to the skin dose when a 10 mm bolus was positioned in the path of a 6 MV X-ray beam when measuring doses under small gaps found below the bolus material using an a radiochromic film and an Attix parallel-plate ionization chamber. They also determined that a 4 mm air gap will reduce dose deposited at the basal layer by approximately 0 to 4% and a 10 mm air gap will reduce dose to the basal cell layer up to 10%. They deduced that for air gaps up to 10mm, at least 90% of maximum dose is still delivered (Butson et al., 2000).

Sroka et al. examined how the increase of dose in water in the build-up region related with the distance of the bolus from the water surface for the applied parameters of X-ray beams. Percentage depth dose measurements were performed using Markus parallel-plate ionization chamber in an automatic blue water phantom for varying field sizes using 6 MV and 15 MV X-ray beams respectively. The bolus used was a water equivalent RW3 slab. They discovered that for all the field sizes and energies investigated, the depth of the maximum dose in the phantom became smaller when the bolus was brought closer to the water surface. They also found out that bolus influence can be neglected when the distance between the bolus and the surface of the blue water phantom distance is equal to 25 cm and 39 cm for 6 MV and 15 MV X-ray beams respectively (Sroka et al., 2010).

2.5 Radiation dosimeters

Rajan and Izweska defines a radiation dosimeter as a device, instrument or system that measures or evaluates, either directly or indirectly, the quantities exposure, kerma, absorbed dose or equivalent dose, or their time derivatives (rates), or related quantities of ionizing radiation (Rajan & Izewska, 2012). The radiation dosimeter is capable of providing a reading that is a measure of the average absorbed dose deposited by ionizing radiation in its sensitive volume. A dosimetry system consists of a dosimeter with a reader. For a radiation dosimeter to function, it must possess at least one physical property that is a function of the dosimetric quantity to be measured and that, with proper calibration, is useful for radiation dosimetry (Rajan & Izewska, 2012).

Due to the steep dose gradient in the buildup region, the radiation dosimeter size should be as small as possible along the incident beam. It is because of this condition extrapolation chambers are the instruments most desired for the measurements (F. M. Khan & Gibbons, 2014). However, these instruments are available in only a few centers and therefore the fixed separation plane parallel ionization chambers are utilized as the alternative. In addition to ionization chambers, thin layers (< 0.5 mm) of TLD material (Rapley, 2006) and radiochromic films (an example being GafChromic films) are available for the measurement of skin dose. The film must first be calibrated within the dose range required before use (Butson et al., 1999; Khan & Gibbons, 2014). GafChromic films, ionization chamber and diode were the choice of dosimeters to be used for this study due to their availability at the facility.

2.5.1 Ionization chambers

They are radiation dosimeters used both in radiotherapy and diagnostic radiology to determine radiation dose (Rajan & Izewska, 2012). Based on the specific requirements, ion chambers are designed in various forms but in general they all have these traits: An ionization chamber is essentially a cavity filled with gas, encompassed by a conductive outer wall and a central collecting electrode and where a high-quality insulator is used as a division between the two to limit the leakage current when is the chamber receives an application of a polarizing voltage. The chamber leakage is further reduced with the provision of a guard electrode which intercepts the leakage current and allows it to flow to ground, bypassing the collecting electrode. The guard electrode also improves charge collection by enhancing field uniformity in the chamber's active/sensitive which is advantageous. Temperature and pressure correction is required for measurements with open air ionization chambers. This correction accounts for the change in the mass of air in the chamber volume as created a result of changes in the ambient temperature and pressure. For surface dose measurements, fixed plate ionization chambers and extrapolation chambers are recommended (Andreo et al., 1995; Khan & Gibbons, 2014; Rajan & Izewska, 2012; Rawlinson et al., 1992).

2.6 Electrometers

They are devices used for measuring small currents (approximately 10^{-9} A or less). It is an operational amplifier with high gain, negative feedback and having a standard resistor or a standard capacitor in the path of the feedback. It used along with an ionization

chamber to measure the chamber current or charge collected over a fixed period of time (Rajan & Izewska, 2012).

2.7 Radiochromic film

Radiochromic film is one of the many dosimeters used for taking measurements. It is a relatively new type of film in radiation therapy with GafChromic film being the most commonly used radiochromic film. GafChromic film types include HD-810, DM-1260, EBT, EBT2, EBT3, MD-55 and MD-55-2 with an effective depth of skin dose measurement at 0.17mm ± 0.03mm. It is a colourless film with a composition which is almost tissue-equivalent (9.0% hydrogen, 60.6% carbon, 11.2% nitrogen and 19.2% oxygen) that changes colour to blue after exposure to radiation (Rajan & Izewska, 2012). Radiochromic films contain a monomer crystal in a gel bound to a Mylar (polyethylene terephthalate) substrate, a special dye that is polymerized when exposed to radiation. When light is absorbed by the polymer, an appropriate densitometer can be utilized to measure the transmission of light through the film. Radiochromic films do not require a developer or a fixer because they are self-developing. Below 50 mGy, the film's response to radiation exposure is not noticeable and therefore the flatbed scanner is incapable of picking up the small changes in film colour (Lewis, 2009). In dosimetry, radiochromic films possess some few advantages over radiographic films. They are easy to use and do not require darkroom facilities, film cassettes or film processing. Radiochromic films are also dose rate independent. In addition, they are insensitive to ambient conditions and have better energy characteristics except for X rays with energies less than or equal to 25 kV (Podgorsak, 2005; Rajan & Izewska, 2012). Radiochromic film is a relative dosimeter and but when appropriate care is taken during calibration and the environmental

conditions are carefully monitored or adjusted, a precision better than 3% can be achieved (Khan & Gibbons, 2014; Rajan & Izewska, 2012). The film is also used for field size alignment and shaping of radiation fields, detecting radiation leakage around the collimator head and positioning of special radiation fields (Niroomand-Rad et al., 1998).

2.7.1 GafChromic EBT3 film

The radiochromic film employed for this work is the GafChromic EBT3 film. It has a dynamic range designed for optimal performance in the dose range of 0.2 to 10 Gy. It is therefore appropriate for several applications in intensity modulated radiotherapy (IMRT), volumetric-modulated arc therapy (VMAT) and brachytherapy. Just like all other radiochromic films, the GafChromic EBT3 film is self-developing and therefore it does not need a developer or a fixer. Some important technical features of the GafChromic film are; it has dynamic dose range of 0.1 Gy to 20 Gy with an optimum dose range of 0.2 Gy to 10 Gy; it can be developed in real time without treatment after exposure; it has a minimal response difference from 100 keV into the megavoltage range; it is near tissue-equivalent; it has a high spatial resolution with the capability of resolving features down to 25 μm or less; it has proprietary new technology which involves incorporating a marker dye in the active layer to enable correction for non-uniformity when making use of multi-channel dosimetry and to decrease visible and ultraviolet light sensitivity; and it offers stability at temperatures up to 60°C.

2.7.2 Configuration and structure of GafChromic EBT3

The film is consists of a 28 μm thick active layer, positioned in the middle of two 125 μm matte-polyester substrates as shown in figure 2.3. The active layer is made up of the active component, a marker dye, stabilizers and other components which gives the film its near energy independent response. The active layer thickness may not exactly be the same for different production lots. Figure 2.3 below shows the structure of GafChromic EBT3 dosimetry film.

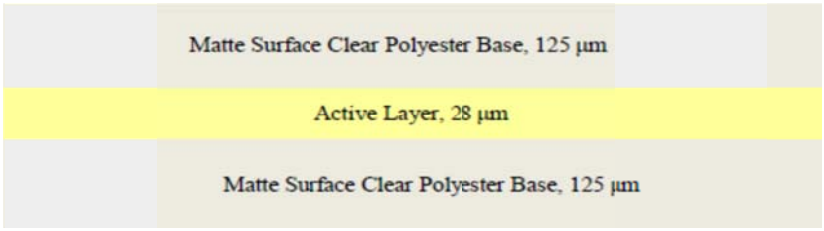

Figure 2.3: Structure of GafChromic EBT3 Dosimetry film.

2.7.3 Medical Applications of Radiochromic films

Radiochromic films when compared to commonly available detectors are relatively insensitive to radiation and because of this lack of sensitivity, they are optimal for dosimetry where high doses are employed (Niroomand-Rad et al., 1998). Radiochromic films have an extensive use in medical applications that range from high dose gamma ray exposures as seen in brachytherapy to low dose clinical assessment in-vivo such as conventional radiotherapy of breast cancer patients (Butson et al., 1999; Stevens et al., 1996).

2.7.3.1 Skin and surface dosimetry

Radiochromic film is a popular choice for dosimetry in radiotherapy due to its low energy dependence, its capability to produce a 2-D dose map which is currently unavailable in other skin dosimeters and its relatively small effective thickness. These applications include in-vivo dosimetry in addition to phantom studies for assessing dose at the skin surface, basal and dermal cell layers, including subcutaneous layers (Niroomand-Rad et al., 1998).

2.7.4 Advantages of GafChromic films

GafChromic films give permanent absolute values of absorbed dose with precision and accuracy that is acceptable. They also provide a larger area for dosimetry; including beam profiles. The film has a higher spatial resolution compared to other radiochromic films. GafChromic films are easy to handle and analyze. They do not require darkrooms or chemical processing because they are insensitive to visible light. They are also water resistant and usable with water phantoms.

2.8 Linear Accelerators (LINACS)

A Linear Accelerator is a device that makes use of high radio-frequency (RF) electromagnetic waves to cause the acceleration of electrons to high energies in a straight path in a special evacuated structure referred to as the accelerating waveguide. The medical linac has a resonating cavity frequency of about 3 billon Hertz and is the most common device that is utilizes external beam radiation to treat cancer (Khan & Gibbons, 2014).

Linacs are normally assembled isocentrically and the operational systems are distributed over five different sections of the machine. These are the modulator cabinet, the gantry, the patient support assembly (treatment table), the gantry stand or support, and the control console. The components that form the main beam are generally grouped into six classes. These are the RF power generation system, injection system, beam transport system, accelerating waveguide, auxiliary system, and the beam collimation and beam monitoring system (Podgorsak, 2005). Figure 2.4 below shows the parts of a medical linac.

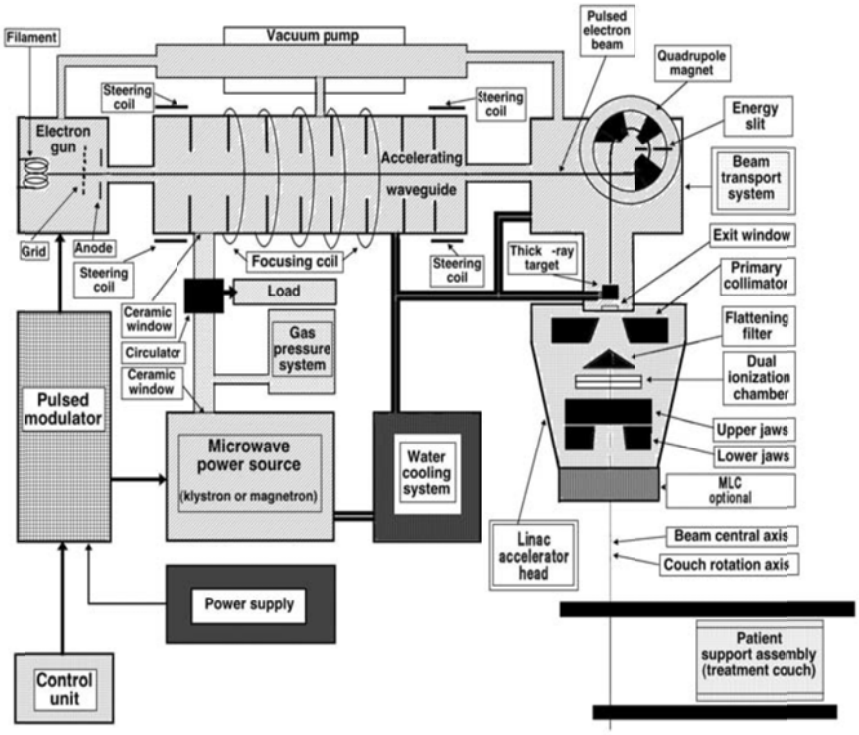

Figure 2.4: Parts of a Medical linac (Ervin B Podgorsak, 2005, pp. 139)

Medical linacs are capable of producing X-ray photon beams of energies within 4 MV to 22 MV. They can also produce electron beams with energy group between 4 MeV and 22

MeV. Linear accelerators are applied in various fields/areas such as medicine, radiography, nuclear fuel breeding, radiation damage neutron source, heavy ion fusion and other possibities. Their applications in these areas have been reviewed by numerous researchers (Cleland & Road, 1984; Hamm, 1988; Hamm, 1990; Knapp, 1976).

Although medical linacs are now the most commonly used megavoltage radiotherapy machines today, the first practical megavoltage therapy machine was the Cobalt-60 (^{60}Co) teletherapy machine developed in the 1950s. The important features of a ^{60}Co teletherapy machine include; a relatively high energy gamma ray emission, a relatively long half-life, a relatively high specific activity and a relatively simple means of production. Medical linacs hold several advantages over ^{60}Co teletherapy machines. One advantage is that a linac can provide mega voltage beam and mega voltage electron beams with a wide range of energies as compared to a ^{60}Co unit, which provides essentially only one gamma ray energy of 1.25 MeV. Linacs also are more complex in design than ^{60}Co machines due to their multimodality capabilities, their control systems have increased the utilization of computer logic and microprocessors, and because of added features which include multileaf collimation, high dose rate modes, electron arc therapy and a dynamic treatment option (dynamic wedges and MLC leaves) (Podgorsak, 2005).

CHAPTER THREE

MATERIALS AND METHODS

3.1 Introduction

The methodologies adopted to evaluate the implications of air gaps on surface dose using calibrated GafChromic EBT3 films and PTW Roos electron chamber are presented in this chapter. Calibration of GafChromic EBT3 films for assessing skin dose with solid water phantom together with the dose measurements using both the GafChromic EBT3 films and the PTW Roos chamber are outlined in this chapter. Dose verification using the RANDO phantom is also captured in this chapter.

3.2 Materials

The materials used in this study include; linear accelerator (LINAC) Elekta Synergy, Superflab bolus, GafChromic EBT3 film, styrofoam sheets, RW3 slab phantom, EPSON Stylus CX5900 flatbed scanner, PTW Roos electron chamber, PTW UNIDOS (Webline) electrometer, RANDO phantom, diode, ImageJ software, barometer and digital thermometer. Some specific materials are presented with details below.

3.2.1 Elekta Synergy Linear Accelerator (LINAC)

The Elekta Synergy Platform Linac as shown in Plate 3.1 was used to produce the megavoltage beams for this study. This linac consists of a standard 80 leaf multi-leaf collimator (MLC) with leaf thickness of 10 mm at isocenter and allows for image guided

radiotherapy (IGRT). The LINAC features an iBEAM evo carbon fibre couch top as well as a fitted motorized wedge. It is able to produce electron beams of 6, 10 and 15 MeV as well as photon beams of 6 and 15 MV. It is capable of delivering isocentric treatment techniques with a high degree of accuracy (Podgorsak, 2005).

Plate 3.1 Elekta Synergy Linear Accelerator (SGMC, Ghana)

3.2.2 Superflab Bolus

The bolus material used for this study was Superflab as shown in Plate 3.2. It is made of synthetic oil gel which makes it very elastic and flabby and prevents it from suffering inelastic strain from normal stresses. Its dosimetric properties have been tested to be superior to polystyrene, which was previously the best material used for making bolus, when using both electron and photon beam energies. The tissue-equivalence of Superflab is also closer than that of polystyrene as it has a specific gravity very similar to water at 1.02. It is known to enhance dose build-up to skin and its design allows it to conform completely to a varying range of uneven surface geometries. Superflab is therefore widely accepted in radiotherapy clinics worldwide (Vyas et al., 2013).

Plate 3.2: Superflab bolus

3.2.3 GafChromic EBT3 film

GafChromic EBT3 film (International Speciality Products, Wayne, NJ) with lot number # 042011601 and dimensions 8×10 inches was used for this work. The dynamic dose range of the film is from 0.1 Gy to 20 Gy. However it has an optimum dose range from 0.2 Gy to 10 Gy and can be used alongside an RGB film scanner for triple-channel dosimetry. For dose range between 0.1 Gy to 6 Gy, the film response is more sensitive when scanning in the red channel, hence the red channel pixel values were used in this work. However above 10 Gy the red channel approaches saturation and the green channel is preferred for taking measurements (León Marroquin et al., 2016). Plate 3.3 shows the GafChromic films cut into small strips.

Plate 3.3: GafChromic EBT3 films (cut)

3.2.4 Styrofoam Sheet

Styrofoam, generically known as extruded polystyrene foam, is one of the most widely used types of plastic today. However the term Styrofoam is also applied to expanded polystyrene foam. Polystyrene foam sheets are very lightweight and they are made up of 5% plastic and 95% air. These sheets are made up of expanded polystyrene beads. Because they are made up of 95% air, the Styrofoam sheets were ideal to be used to mimic air gaps under the bolus (Karabedian & Blackwelder, 1992). Plate 3.4 shows a sample of the Styrofoam sheets used for this study.

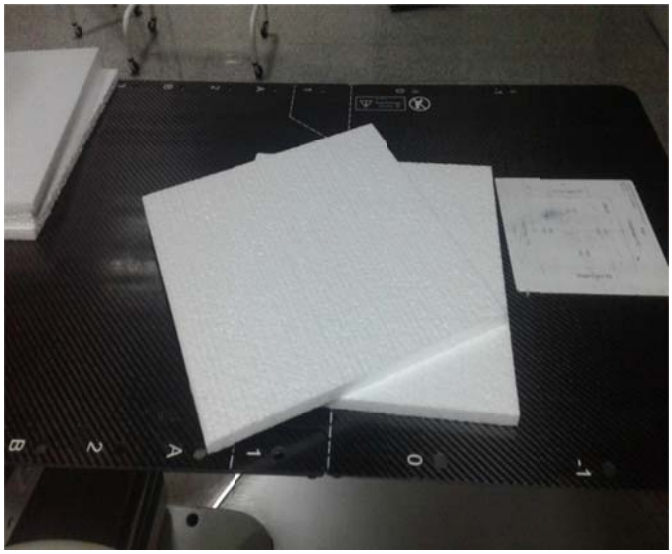

Plate 3.4: Polystyrene foam sheets popularly known as Styrofoam sheets.

3.2.5 RW3 Slab Phantom

The RW3 phantom (PTW, Freiburg, Germany) was used in the calibration of the GafChromic films and for dose measurements using both the GafChromic films and the ion chamber. It is designed using water-equivalent RW3 material (Goettingen White Water) with thickness tolerance of ± 0.1 mm. It is suitable for dosimetry for high energy electrons and photons and it also makes it possible for depth dose measurements and monitor calibrations be performed in a solid state phantom. Measuring depths can be varied in increments of 1 mm up to 30 cm. The surface area of each slab is 30 × 30 cm^2 (Christ, 1995). Plate 3.5 shows the RW3 slab phantom used for this study.

Plate 3.5: RW3 slab phantom with a cut GafChromic EBT3 film placed on it.

3.2.6 EPSON Stylus CX5900 flatbed scanner

The Epson Stylus CX5900 flatbed scanner (Plate 3.6) was used to scan the GafChromic films. Epson scanners have been proven to be of high quality when it comes to film dosimetry. The scanner provides sensitive response for GafChromic films at doses up to 8 Gy in the red colour channel (Ferreira, Lopes, & Capela, 2009).

Plate 3.6: EPSON Stylus CX5900 flatbed scanner.

3.2.7 PTW Roos Electron Chamber

The PTW (Freiburg, Germany) Roos Electron Chamber TM34001 (Plate 3.7) was used in this work. It has a serial number S/N 002017. It was used with the RW3 slab phantom to measure the doses for the varying air gaps and field sizes introduced in this study. It has a vented sensitive volume of 0.35 cm^3 therefore readings obtained from using the chamber need to be corrected for factors like temperature, humidity and pressure that affect air density (Niroomand-Rad et al., 1998).

Plate 3.7: PTW Roos Electron Chamber.

3.2.8 PTW UNIDOS (Webline) Electrometer

The PTW UNIDOS (Webline) electrometer as shown in Plate 3.8 with serial number S/N 000590 was used in this study. It was used to quantify charges that had been collected with the Roos chamber. Measurements were recorded in nanocoulombs (nC). The measured values were then corrected for temperature and pressure variations (Niroomand-Rad et al., 1998).

Plate 3.8: PTW UNIDOS (Webline) Electrometer.

3.2.9 RANDO Phantom

The RANDO phantom was used in this work to mimic clinical conditions as these phantoms are tissue equivalent and are designed to simulate the physical characteristics

of humans. The RANDO phantom as shown in Plate 3.9 is made of plastic tissue-equivalent materials and natural skeletal tissue. It is divided into 36 sections with every section bearing a number from 0 to 35. They provide detailed mapping of dose distribution that is key in the analysis of radiotherapy treatment plans. Scalzetti et al. stated that, "It is straightforward to make dose measurements at any given point in the RANDO phantom". Dose measurements are obtained either by using film or individual dosimeters with holes in each section of the phantom except 0 and 35 for the placement of dosimeters (Scalzetti et al., 2008).

Plate 3.9: RANDO phantom.

3.2.10 Diodes

Diodes were used in this study to measure doses at d_{max} on the RANDO phantom. They are smaller in size and more sensitive than typical ionisation chambers. They are often used for measurement of doses at depth in electron beams and are useful for measurements in phantoms (Podgorsak, 2005). Diodes are mostly used in radiotherapy treatment to measure the dose the patient is receiving in "real time" with the help from a diode reader. Plate 3.10 shows the diode used for taking measurements.

Plate 3.10: Diode taped to Superflab bolus.

3.2.11 ImageJ Software

The ImageJ software (plate 3.11) was used to obtain mean pixel values from the scanned GafChromic films. ImageJ is an open source image processing program designed for scientific multidimensional images. It is highly extensible and can be used to perform a wide range of tasks like solving many image processing and analysis problems. ImageJ can calculate area and pixel value statistics when a portion of the image is selected by the user. It is capable of analysing 8-bit, 16-bit and 32-bit images. It is capable of reading many image formats including GIF, BMP, TIFF, DICOM, JPEG, FITS and "raw" (Bailer, 2006).

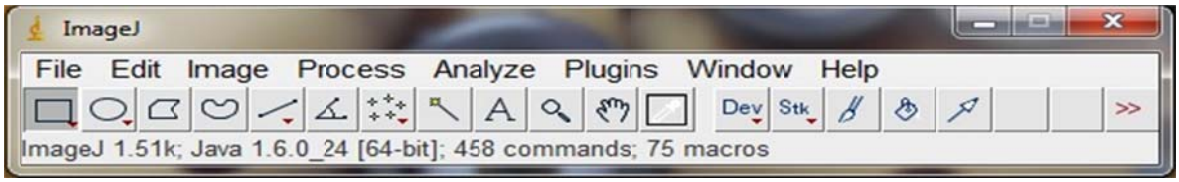

Plate 3.11: ImageJ Software Interface.

3.2.12 Digital Thermometer

The digital thermometer shown in plate 3.12 was used to measure the temperature in the treatment room. The temperature was measured in degree Celsius (°C) and was used in the determination of the temperature and pressure correction factor.

Plate 3.12: Thermometer

3.2.13 Barometer

The barometer (plate 3.13) was used to measure the pressure in the treatment room. The pressure was measured in kilopascal (kPa) and was used in the determination of the temperature and pressure correction factor.

Plate 3.13: Barometer

3.3 Experimental Method

3.3.1 Calibration of GafChromic EBT3 Films

Precautionary measures specified in TG-55 (Niroomand-Rad et al., 1998) concerning the handling of radiochromic films were observed. The films were carefully handled and prepared on a clean surface to avoid dirt and fingerprints. The orientation of the film was

marked after it was removed from the lot to reduce inaccuracies in the optical densities to be measured and subsequently the measured doses as a result of orientation effects.

The film set to be used for the calibration was exposed in a phantom composed of 30×30 cm^2 sheets of the RW3 slab phantom. The 10×10 cm^2 was selected and set at the isocenter and the SSD set at 100cm. The GafChromic films were cut into small pieces with dimensions of 2×3 cm^2 and labelled according to the respective doses they were to be irradiated with. They were then placed between the slabs of the RW3 phantom positioned perpendicular to the beam central axis at d_{max} (1.6 cm and 2.5 cm for 6 MV and 15 MV respectively). The films were exposed to uniform radiation at dose levels of 0, 20, 40, 160, 240, 320, 400 and 500 cGy for both photon beam energies of 6 MV and 15 MV.

The exposed films were allowed to stay for 14 days for post irradiation development (coloration) before being scanned using the EPSON Stylus CX5900 flatbed scanner. Scanning of the films was done in transmission mode with 48 bit colour mode and a resolution of 72 dpi. No colour corrections were applied. The scanned images were saved in TIFF format and ImageJ 1.46r was used to analyse the images. The data were analysed by splitting image data of the film into blue, green and red colour channels. For every image scanned and colour channel, a region of interest (ROI) covering a sizeable portion of the scanned image at the field centre was selected to generate the mean pixel value. However selection of the ROI was carefully made to avoid possible film artefacts which could change the pixel values. The responses of the images after they were read by the ImageJ software were recorded. These values were plotted to give calibration functions for both 6 MV and 15 MV photon beams.

3.3.2 Measurement of skin dose using GafChromic EBT3 film

3.3.2.1 Setup and film irradiation

Skin dose measurements were carried out using GafChromic EBT3 films. Precautionary measures specified in TG-55 (Niroomand-Rad et al., 1998) concerning the handling of radiochromic films were observed. GafChromic EBT3 films were cut into small pieces with dimensions of 2×3 cm^2 each and were labelled A and B for easy identification. Using the isocentric technique, film set A was positioned on the surface of the phantom and film set B at d_{max}. The SSD used in the set-up was 100cm. This set-up was done for both 6 MV and 15 MV. Plate 3.14 below shows the set up for surface dose measurements without the application of bolus using GafChromic EBT3 film.

Plate 3.14: Set up for measuring surface dose without bolus using GafChromic EBT3 film.

The air gap between the surface of the phantom and the bolus was achieved and subsequently adjusted using Styrofoam sheets. Dose measurements were taken with air

gaps of 1 cm, 2cm, 3 cm, 4 cm and 5 cm as shown in the set up in Plate 3.15. Measurements without bolus and with the bolus placed directly on top of the solid water phantom were also performed. Measurements were taken for field sizes of 5×5 cm^2, 10×10 cm^2, 15×15 cm^2 and 20×20 cm^2. All the films were exposed to radiation dose of 1 Gy. Bolus thickness of 0.5 cm was used for 6 MV photon beams and 1.0 cm for 15 MV photon beams.

Plate 3.15: Set up for measuring surface and d_{max} dose with 1 cm bolus (15 MV photon beam) using GafChromic EBT3 film and Styrofoam sheets to act as a spacer (air gap).

The film sets of A and B were kept in envelopes that were labeled with the energy, the field size and bolus to phantom surface distance used. The exposed films together with those that were not exposed were kept for 14 days to allow for maximum post irradiation coloration.

3.3.2.2 Scanning of irradiated dose films

After 14 days, the exposed films were removed and scanned using EPSON Stylus CX5900 flatbed scanner. The lid of the scanner and the scanner itself was cleaned to remove any dirt and the films were handled with care to minimize errors. Scanning of the films was done in transmission mode with 48 bit colour mode and a resolution of 72 dpi. The films were placed in landscape mode for scanning as done during the calibration due to the orientation of the film having an effect on the on the film response. All film scans were performed using the same scanner under the same settings on the same day to minimize the scanner variability.

3.3.2.3 Reading of the exposed films

The exposed films from the Elekta Synergy linear accelerator were read using ImageJ 1.46r as indicated in figure 3.1 by splitting the film image data into the individual colour channels (blue, green, and red).

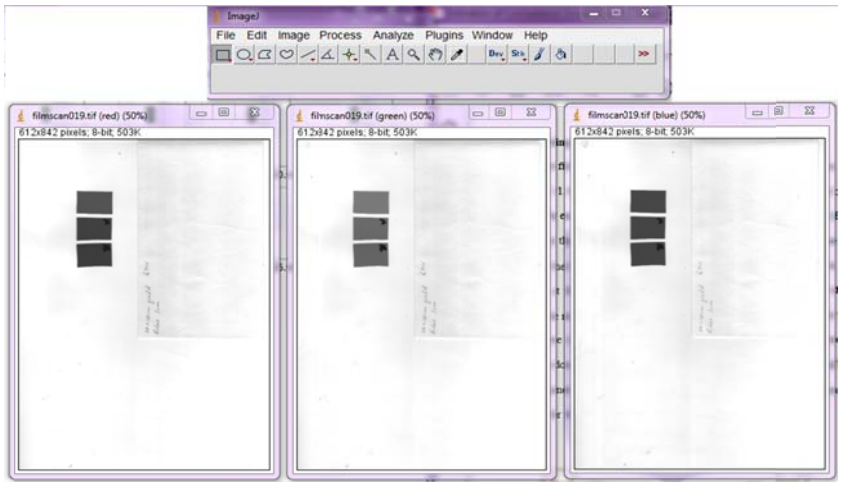

Figure 3.1: ImageJ splitting scanned films into the individual RGB channels.

For every scanned image and colour channel, a region of interest (ROI) covering a sizeable portion of the scanned image at the field centre was selected (figure 3.2) to obtain the mean pixel value.

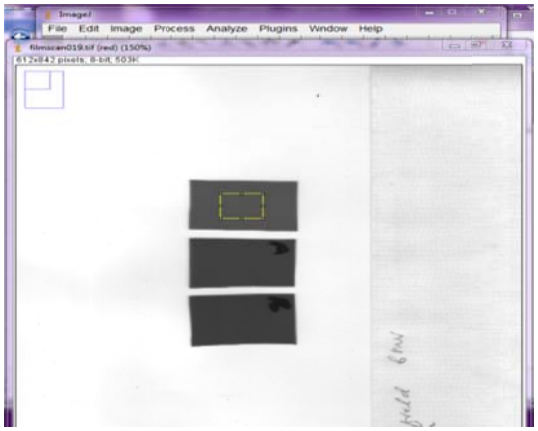

Figure 3.2: ROI selected to obtain pixel value.

However selection of the ROI was carefully made to avoid possible film artefacts which could change the pixel values. The response values of the images after they were read by the ImageJ software were recorded and using the calibration equation, these readings were converted to doses.

The response of the GafChromic EBT3 film is characterized by the net optical density due to the color change in response to radiation exposure (León Marroquin et al., 2016).

Equation 3.1 shows the relationship between the intensity (I) and the net optical density:

$$Net\ Optical\ Density = -log_{10}\ \frac{I}{I_0} \quad \text{.....3.1}$$

Where I and I_0 are the reading for the exposed and unexposed film piece, respectively (León Marroquin et al. , 2016).

3.3.3 Measurement of skin dose using PTW Roos Chamber (Parallel plate)

The RW3 phantom was set up on the Elekta Synergy linear accelerator couch, perpendicularly along the beam central axis. A PTW Roos electron chamber of 0.35 cc measuring volume along with a PTW UNIDOS (Webline) electrometer were used to collect and measure charges collected respectively.

Measurements of dose to the surface were taken with the Roos chamber positioned at the surface of the RW3 phantom with SSD of 100 cm and radiation dose of 1 Gy. The air gap between the surface of the phantom and the bolus was achieved and subsequently adjusted using Styrofoam sheets. Dose measurements were taken with air gaps of 1 cm, 2cm, 3 cm, 4 cm and 5 cm. Measurements without bolus and with the bolus placed directly on top of the solid water phantom were also performed. Measurements were taken for field sizes of 5×5 cm^2, 10×10 cm^2, 15×15 cm^2 and 20×20 cm^2. Bolus thickness of 0.5 cm was used for 6 MV photon beams and 1.0 cm for 15 MV photon beams. Charges were collected by the Roos chamber and measured using the electrometer. Three successive readings were taken for each measurement and their average values determined and recorded. The initial and final temperatures and pressures were also recorded using a thermometer and a barometer respectively. These measured values were then corrected for temperature and pressure and subsequently converted to doses.

From TRS-398 (IAEA, 2000), the absorbed dose was calculated using the equation:

$$D = R_{cor} \times N_{D,W} \times k_Q \quad \text{..... 3.2}$$

Where R_{cor} is the corrected ion chamber reading, $N_{D,W}$ is the calibration factor and k_Q is beam quality correction factor. R_{cor} is obtained from the equation:

$$R_{cor} = R_{raw} \times P_{T,P} \quad \text{..... 3.3}$$

Where R_{raw} is the raw ion chamber reading and $P_{T,P}$ is the temperature and pressure correction factor.

The temperature and pressure correction,$P_{T,P}$ at different conditions is given by:

$$P_{T,P} = \left(\frac{101.33}{P}\right) \times \left(\frac{273.2+T}{273.2+22.0}\right) \quad \text{..... 3.4}$$

Where P is the pressure in kilopascal (kPa) and T is the temperature in degree Celsius (°C).

3.3.4 Dose verification using RANDO phantom

Scanning of the RANDO phantom using the Siemens SOMATOM Emotion 16 CT-scanner and the Oncentra Masterplan v4.3 Treatment Planning System (TPS) was used to plan doses to be delivered to the RANDO phantom with the thorax being the treatment site. The treatment position of the phantom (Plate 3.16) was head first supine. Isocentric setup was used for both 6 MV and 15 MV. Monitor units to be delivered by the linac was set at 200 MU and 100 MU for 6 MV and 15 MV photon beams respectively. Bolus ID was set at 0.5 cm for 6 MV and 1 cm for 15 MV. The field size set for both 6 MV and 15 MV was 10×10 cm^2. A diode was positioned on the surface of the RANDO phantom at the thoracic region to measure doses at d_{max} for both 6 MV and 15 MV without a bolus. Measurements with the bolus positioned directly on the surface of the RANDO phantom and with air gaps of 1 cm and 2 cm were also performed. The bolus thicknesses used for 6 MV and 15 MV were 0.5 cm and 1 cm respectively.

Plate 3.16: Set up for measuring d_{max} (2.5 cm) dose with 1 cm bolus (15 MV photon beam) using diode and Styrofoam sheets to act as a spacer (air gap).

CHAPTER FOUR

RESULTS AND DISCUSSION

4.1 Introduction

This chapter presents the analysis of the results obtained and discusses the implications of the results. Analysis was made on the calibration of the GafChromic films and measured surface dose both from the GafChromic film and the ion chamber.

4.2 Calibration curves

Determination of doses retrieved by scanning GafChromic films can only be done by first obtaining the calibration curves. The calibration curves were obtained by plotting a graph of the measured optical densities against dose as displayed in Figure 4.1 and Figure 4.2. Table 4.1 and Table 4.2 below show the absorbed dose and its corresponding measured optical density for the various colour channels for the 6 MV and 15 MV photon beam respectively. Appendix B shows the mean pixel values for the blue, green and red channels.

Table 4.1: Prescribed doses and the corresponding optical densities for the various colour channels using 6 MV.

Dose (Gy)	Optical Density Blue Channel	Optical Density Green Channel	Optical Density Red Channel
0.0	0.000	0.000	0.000
0.2	0.010	0.030	0.044
0.4	0.011	0.043	0.077
0.8	0.019	0.072	0.120
1.6	0.035	0.123	0.183
2.4	0.053	0.174	0.233
3.2	0.065	0.214	0.260
4.0	0.083	0.256	0.292
5.0	0.096	0.294	0.308

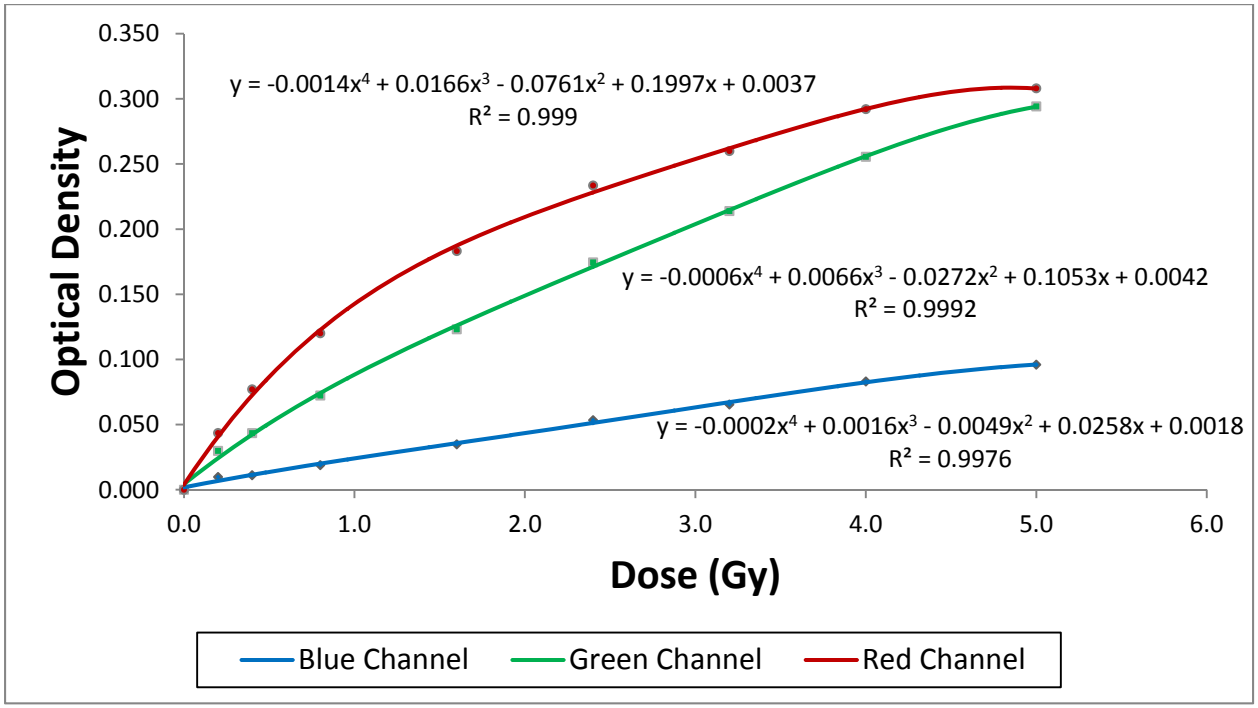

Figure 4.1: Calibration curves of the various colour channels for 6 MV photon beam.

Table 4.2: Prescribed doses and the corresponding optical densities for the various colour channels using 15 MV.

Dose (Gy)	Optical Density Blue Channel	Optical Density Green Channel	Optical Density Red Channel
0.0	0.000	0.000	0.000
0.2	0.014	0.026	0.055
0.4	0.016	0.040	0.077
0.8	0.028	0.078	0.136
1.6	0.041	0.126	0.198
2.4	0.055	0.169	0.243
3.2	0.072	0.215	0.274
4.0	0.090	0.255	0.302
5.0	0.103	0.293	0.320

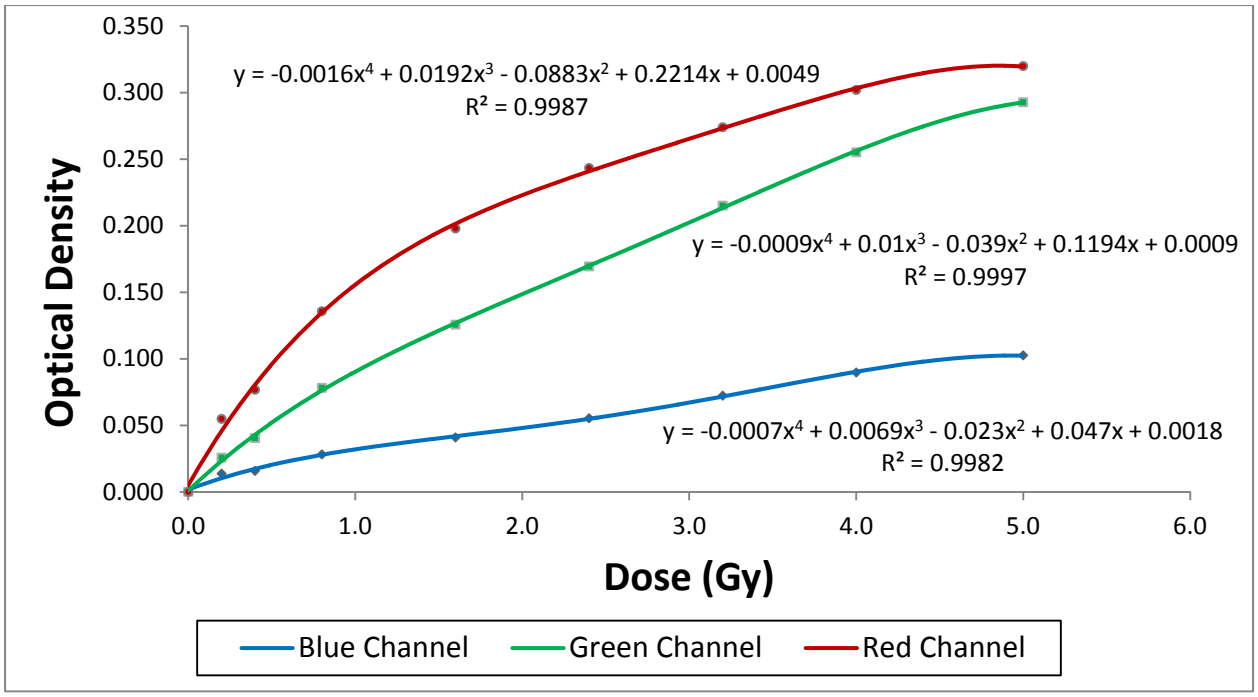

Figure 4.2: Calibration curves of the various colour channels for 15 MV photon beam.

The calibration curve of the red channel was used in determining the doses deposited in the GafChromic films as the film response is more sensitive within the range of 0 to 6 Gy

in the red channel (León Marroquin et al., 2016). A graph of dose against optical density was plotted to obtain the calibration functions to be used to determine the dose deposited in the films for both 6 MV and 15 MV photons as shown in Figure 4.3 and Figure 4.4 below.

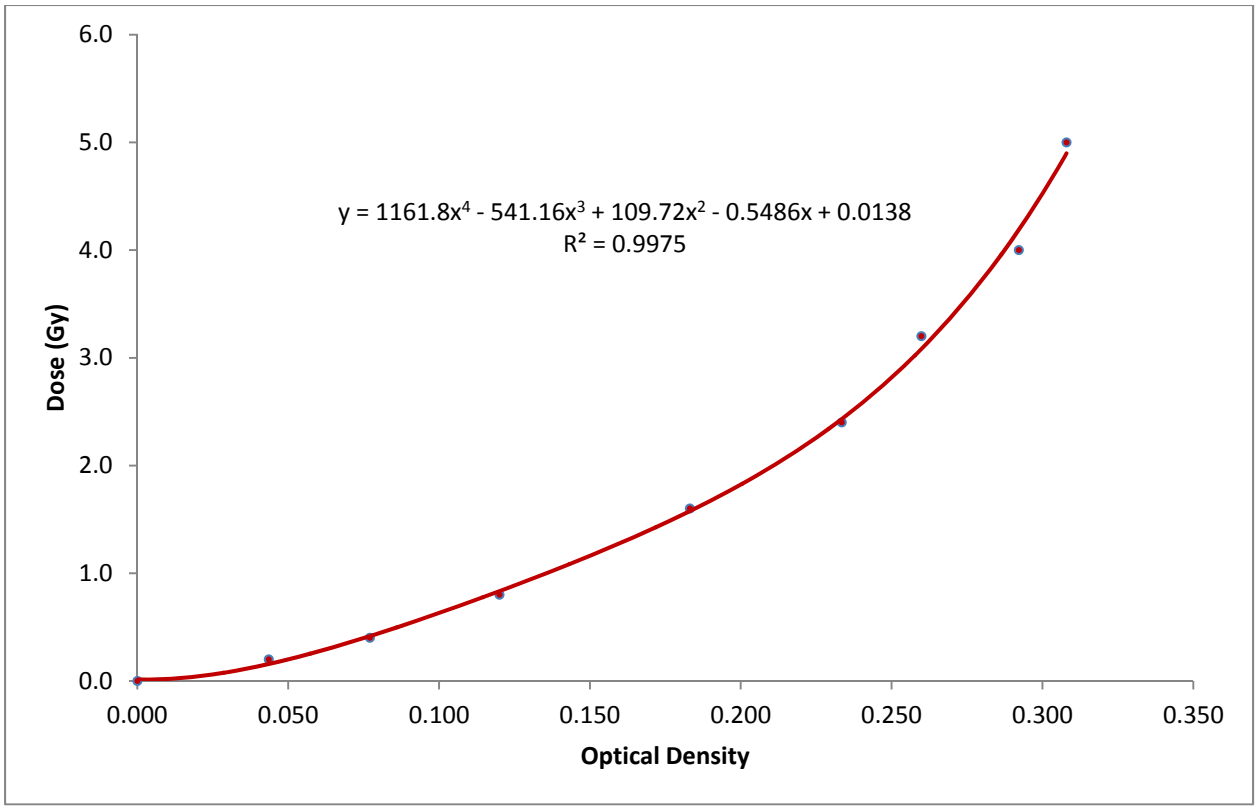

Figure 4.3: Calibration graph of 6 MV photon beam using the red channel

The calibration equation obtained from figure 4.3 for converting the optical densities into absorbed dose for measurements using 6 MV photon beam is given as:

$$y = 1161x^4 - 541.16x^3 + 109.72x^2 - 0.5486x + 0.0138 \quad \text{.....4.1}$$

with regression $R^2 = 0.9975$.

The associated mean error in the calibration function was about 2%.

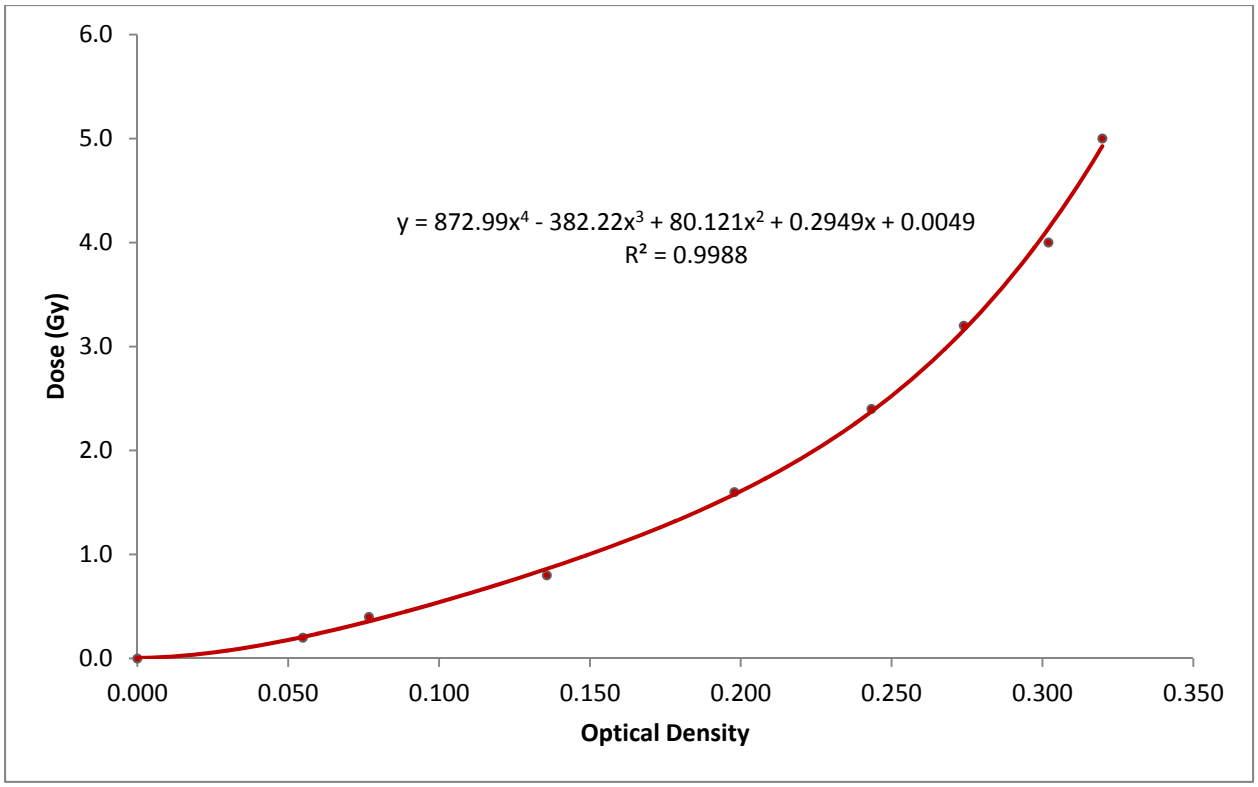

Figure 4.4: Calibration graph of 15 MV photon beam using the red channel

The calibration equation obtained from figure 4.4 for converting the optical densities into absorbed dose for measurements using 15 MV photon beam is given as:

$$y = 872.99x^4 - 382.22x^3 + 80.121x^2 - 0.2949x + 0.0049 \quad \text{.....4.2}$$

with regression $R^2 = 0.9988$.

The associated mean error in the calibration function was about 7%.

4.3 Measured surface doses using GafChromic EBT3 film

Surface dose measurements using the GafChromic EBT3 film were taken for open field (no bolus), bolus placed directly on the RW3 slab phantom and for varying air gaps of 1 cm, 2 cm, 3 cm, 4 cm and 5 cm between the bolus and the phantom. The field sizes used for the measurements were 5×5 cm^2, 10×10 cm^2, 15×15 cm^2 and 20×20 cm^2. Table 4.3 and Table 4.4 show the surface doses for 6 MV and 15 MV photon beams respectively with bolus thickness of 0.5 cm used for 6 MV and bolus thickness of 1 cm used for 15 MV. Figure 4.3 and Figure 4.4 are plots of the surface dose against bolus-to-surface distance for 6 MV and 15 MV respectively. Appendix C shows the mean pixel values and the optical densities for the various air gaps and field sizes for both 6 MV and 15 MV.

Table 4.3: Measurements of dose to the surface for 6 MV using GafChromic film.

Distance of Bolus from Surface (cm)	5 x 5 cm^2 field (Gy)	10 x 10 cm^2 field (Gy)	15 x 15 cm^2 field (Gy)	20 x 20 cm^2 field (Gy)
Open	0.40	0.44	0.50	0.58
0	0.84	0.89	0.91	0.99
1	0.82	0.88	0.92	0.99
2	0.74	0.89	0.96	0.97
3	0.73	0.87	0.96	0.96
4	0.66	0.86	0.94	0.99
5	0.65	0.84	0.97	0.96

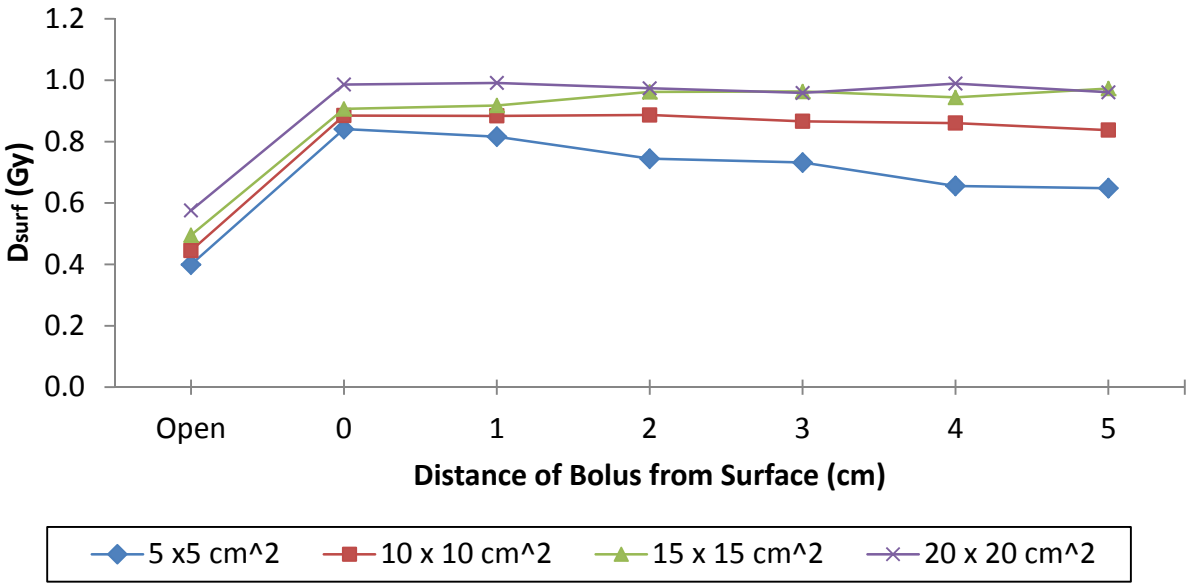

Figure 4.5: Variation of surface dose with air gaps for varying field sizes for 6 MV using GafChromic EBT3 film.

Table 4.4: Measurements of dose to the surface for 15 MV using GafChromic film.

Distance of Bolus from Surface (cm)	5 x 5 cm^2 field (Gy)	10 x 10 cm^2 field (Gy)	15 x 15 cm^2 field (Gy)	20 x 20 cm^2 field (Gy)
Open	0.22	0.28	0.38	0.45
0	0.82	0.91	0.93	1.01
1	0.75	0.88	0.96	0.99
2	0.71	0.88	0.95	1.01
3	0.63	0.84	0.94	1.03
4	0.58	0.82	0.93	1.02
5	0.52	0.76	0.90	1.06

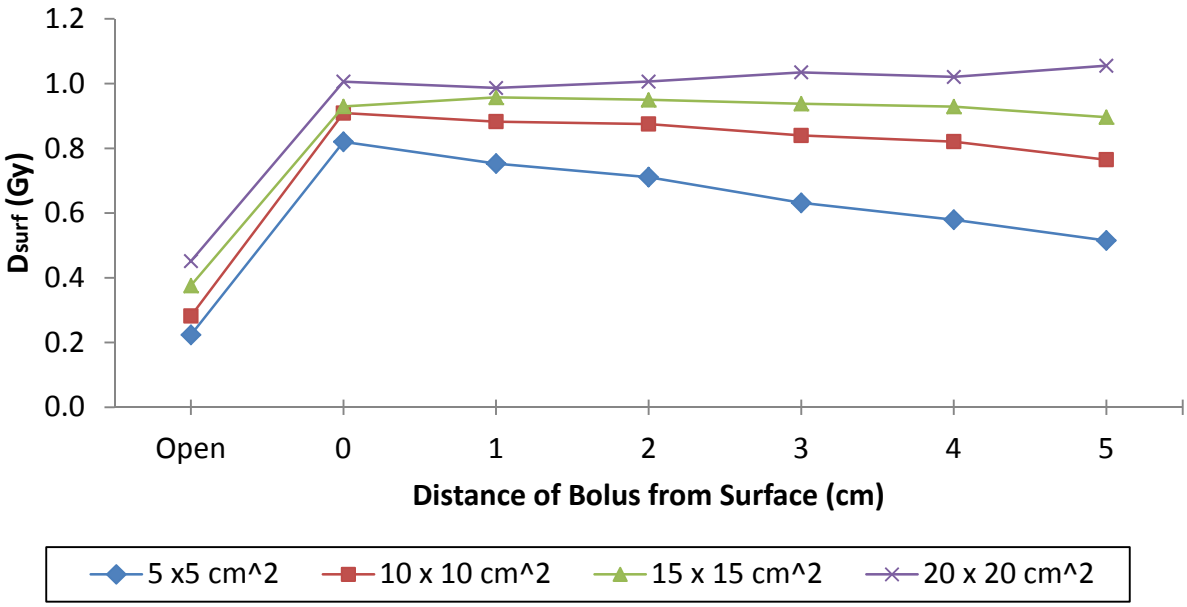

Figure 4.6: Variation of surface dose with air gaps for varying field sizes for 15 MV using GafChromic EBT3 film.

4.4 Measured surface doses using Roos chamber

Surface dose measurements using the Roos chamber were taken for open field (no bolus), bolus positioned directly on the RW3 slab phantom and for varying air gaps of 1 cm to 5 cm with increments of 1 cm between the bolus and the phantom. The field sizes used for the measurements were 5×5 cm^2, 10×10 cm^2, 15×15 cm^2 and 20×20 cm^2. Table 4.5 and Table 4.6 show the surface doses for 6 MV and 15 MV photon beams respectively with bolus thickness of 0.5 cm used for 6 MV and bolus thickness of 1 cm used for 15 MV. Figure 4.5 and Figure 4.6 are plots of the surface dose against bolus-to-surface distance for 6 MV and 15 MV respectively. Appendix A shows the conversion of all chamber reading to doses.

Table 4.5: Measurements of dose to the surface for 6 MV using ion chamber.

Distance of Bolus from Surface (cm)	5 x 5 cm^2 field (Gy)	10 x 10 cm^2 field (Gy)	15 x 15 cm^2 field (Gy)	20 x 20 cm^2 field (Gy)
Open	0.38	0.45	0.51	0.57
0	0.82	0.88	0.93	0.97
1	0.80	0.89	0.93	0.98
2	0.76	0.89	0.94	0.98
3	0.72	0.88	0.94	0.99
4	0.67	0.87	0.94	0.99
5	0.65	0.85	0.94	0.99

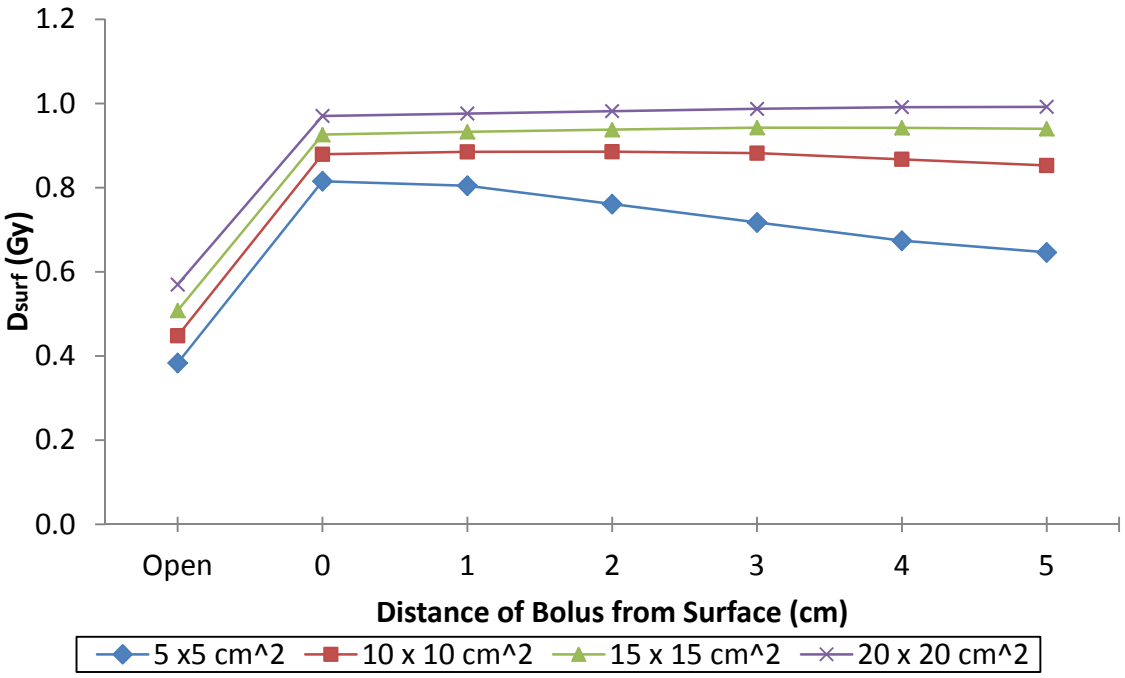

Figure 4.7: Variation of surface dose with air gaps for varying field sizes for 6 MV using ion chamber.

Table 4.6: Measurements of dose to the surface for 15 MV using ion chamber.

Distance of Bolus from Surface (cm)	5 x 5 cm^2 field (Gy)	10 x 10 cm^2 field (Gy)	15 x 15 cm^2 field (Gy)	20 x 20 cm^2 field (Gy)
Open	0.22	0.30	0.38	0.46
0	0.79	0.88	0.94	0.99
1	0.76	0.88	0.95	1.00
2	0.70	0.87	0.95	1.00
3	0.63	0.85	0.94	1.00
4	0.57	0.82	0.93	1.00
5	0.53	0.79	0.92	1.00

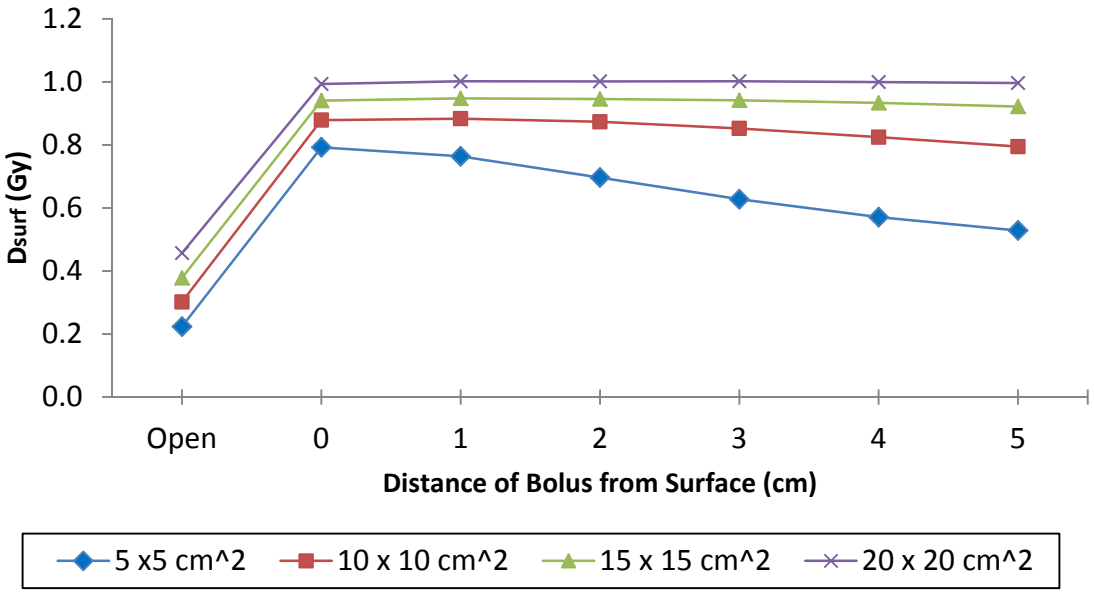

Figure 4.8: Variation of surface dose with air gaps for varying field sizes for 15 MV using ion chamber.

4.5 Discussion of results obtained from GafChromic EBT3 film and Roos chamber measurements

The introduction of the bolus increased the surface dose for all beam energies and all field sizes. This is because the skin sparing effect is removed when the bolus is introduced and therefore the maximum dose is deposited closer to the surface. For instance, for the ion chamber, dose to the surface for the 5×5 cm^2 field size increased by 61% and 72% with the introduction of the bolus when using beam energies of 6 MV and 15 MV respectively. This effect was also recorded by Butson et al. when surface dose recorded with the introduction of a 10 mm bolus increased to 98% and 99% of the maximum dose opposed to 14% and 21% of the maximum dose respectively without the bolus (Butson et al., 2000). Lee et al. discovered that with the introduction of the "bolus effect" as a result of presence of the thermoplastic shell, there was an average increase of dose deposited at the surface of about 18% (Lee et al., 2002). Hsu et al. also acknowledged that the bolus effect was large with an increment of up to 82% when the 2 mm fine mesh Aquaplast was employed (Hsu et al., 2008). Also because there is more skin sparing in higher megavoltage beams than in lower megavoltage beams, the surface doses measured for 6 MV was greater than that of 15 MV for the open beam.

Surface doses also increased as the field size was made larger. For example, for the GafChromic film using 6 MV, the surface dose measured for a field size of 5×5 cm^2 with a bolus-to-skin distance of 2 cm was 0.74 Gy but it increased to 0.97 Gy when the field size was increased to 20×20 cm^2 with the same air gap kept constant. Ignatius in his study also recorded increasing surface doses with increasing field sizes (Ignatius, 2015). This is

because there is more electron contamination as a result of scatter radiation when the field size is increased and therefore a higher dose is deposited at the surface.

Generally, as the air gap increased, the surface dose decreased. However this phenomenon was only seen for small field sizes. Field sizes above 10×10 cm^2 did not show any significant change with increasing air gaps as the surface doses showed very little variation. For instance, for surface doses measured using the ion chamber, the surface dose for the 5×5 cm^2 field reduced by 21% and 33% with a 5 cm air gap for 6 MV and 15 MV respectively. However for 20×20 cm^2 field, the change was negligible with only a 2% and 1% increase in surface dose recorded for both 6 MV and 15 MV respectively. This agrees with the study done by Khan et al. (2013) where it was discovered that for a field size of 5×5 cm^2, the dose to the surface reduces by 34% and 30% with a 5 cm air gap for 6 MV and 10 MV respectively when a bolus of thickness 1 cm was used. Khan's study also observed negligible change in the surface dose for field sizes above 10×10 cm^2 (Khan et al., 2013). This effect is seen because of loss of scatter radiation and secondary electrons from the bolus and other materials in the path of the beam in smaller field sizes as the air gap between the bolus and the surface of the phantom increases. Large field sizes are not affected because they are still able to contain a large amount of scatter radiation and secondary electrons within their field even as the air gap increases. Appendix D shows the percentage difference in measured doses using the GafChromic EBT3 film and the Roos Chamber.

4.6 Measured doses at d_{max} from dose verification using RANDO phantom

Table 4.7 and Table 4.8 below show the results obtained from using the diode to measure doses at d_{max} for 6 MV and 15 MV respectively. Bolus thicknesses used for 6 MV and 15 MV photon beams were 0.5 cm and 1 cm respectively. The percentage deviation between the planned dose and dose delivered for 6 MV and 15 MV photon beams were 4% and 5% respectively which fall within ICRU recommendations (ICRU, 1976).

Table 4.7: Dose measurements at d_{max} (1.6 cm) for 6 MV photon beam using diode.

TPS calculated dose (Gy)	No bolus (Gy)	Bolus present (Gy)	Air gap of 1 cm (Gy)	Air gap of 2 cm (Gy)	Percentage deviation (%)
2.36	2.46	2.48	2.54	2.59	4.07

Table 4.8: Dose measurements at d_{max} (2.5 cm) for 15 MV photon beam using diode.

TPS calculated dose (Gy)	No bolus (Gy)	Bolus present (Gy)	Air gap of 1 cm (Gy)	Air gap of 2 cm (Gy)	Percentage deviation (%)
1.14	1.20	1.22	1.26	1.30	5.00

For both 6 MV and 15 MV, the dose at d_{max} for the beam energy increased as air gap under the bolus increased. This is in agreement with what Khan et al. (2013) observed. They observed that as bolus is placed closer to the phantom surface, the depth at which the maximum dose is deposited for both 6 MV and 10 MV becomes increasingly shallower (Khan et al., 2013). Sroka et al. also observed that as the bolus-to-water surface became smaller, the depth of the maximum dose in the phantom became smaller as well for all fields and energies investigated and conversely, when a tissue-equivalent slab is

moved up from the water surface, the depth in the phantom at which the maximum dose is deposited increases (Sroka et al., 2010). The results show that when the standard d_{max} is kept for both beam energies, the doses increases as the air gap between the bolus and the RANDO phantom becomes larger. This is because as the air gaps increases, the depth at which the maximum dose is deposited shifts further away from the surface and deeper into the phantom and the surface dose decreases accordingly. Conversely, as the air gaps decreases, the depth at which the maximum dose is deposited shifts closer to the surface and therefore the dose to the surface increases.

CHAPTER FIVE

CONCLUSION AND RECOMMENDATIONS

5.1 Conclusion

For both 6 MV and 15 MV, surface doses increased significantly with the introduction of the bolus. Also, due to more skin sparing in 15 MV than 6 MV, surface doses recorded for the 6 MV photons were generally higher than doses measured for the 15 MV photons especially for smaller field sizes. As the bolus-to-surface distance increased, the doses recorded at the surface decreased. This decrease however was seen for the field sizes that were small. For field sizes that were larger, the change in dose to the surface due to change in air gap was negligible. Dose to the surface for 5×5 cm^2 field decreased by 21% and 33% with a 5 cm air gap for 6 MV and 15 MV respectively compared to 20×20 cm^2 field, where the change was negligible with only a 2% and 1% increase in surface dose recorded for beam energies of 6 MV and 15 MV respectively when the ion chamber was employed. The field size of 5×5 cm^2 showed the most variation of surface dose with changing air gaps showing that change in skin dose as a result of air gaps is only significant for small field sizes.

The dose verification using the anthropomorphic phantom showed that when the standard d_{max} is kept for both beam energies, the measured dose at that depth (1.6 cm for 6MV and 2.5 cm for 15 MV) increased as the air gap between the bolus and the RANDO phantom became larger.

Clinically, air gaps are regarded to be mostly small air pockets and the free electrons produced in the bolus material are mostly forward scattered; leaving the bolus and

traversing through the air gap to reach the surface of the skin and deliver dose with only a small percentage scattered. Therefore the presence these air gaps under the bolus should not cause a significant reduction in tumor control although they should be avoided where possible (Butson et al., 2000).

5.2 Recommendations

5.2.1 Radiation Oncology Personnel

a. Special attention should be given to air gaps when field sizes used are small and there is a great variation of surface contours or when the bolus covers a small area.
b. Custom boluses can be developed for use in radiotherapy (example: at SGMC) as they conform to the patient's body contours and eliminate variations.

5.2.2 Research Community

a. Bolus of the same thickness should be used to assess the effect of radiation beams of different energies on the surface dose when air gaps are introduced.
b. Dose verification should be done using a custom bolus and GafChromic films to measure doses at the surface.
c. PDD measurements should also be done to assess the impact of air gaps on doses beyond the skin surface.

REFERENCES

Almond, P., Van Roosenbeek, E., Browne, R., Milcamp, J., & Williams, C. B. (1970). Variation in the position of the central axis maximum build-up point with field size for high-energy. *The British Journal of Radiology*, *43*(516), 911.

Andreo, P., Almond, P. R., Mattsson, O., Nahum, A. E., & Roos, M. (1995). HIGH-ENERGY ELECTRON AND PHOTON BEAMS . Report by a Consultants ' Group to the. *IAEA Technical Report Series*, *TRS-381*(December), 1–143.

Bailer, W. (2006). Writing ImageJ Plugins — A Tutorial. *Applied Sciences*, 1–57. https://doi.org/10.1016/j.agee.2005.08.028

Baskar, R., Lee, K. A., Yeo, R., & Yeoh, K.-W. (2012). Cancer and radiation therapy: current advances and future directions. *International Journal of Medical Sciences*, *9*(3), 193.

Bentel, G. C. (1995). *Radiation Therapy Planning* (2nd ed.). McGraw-Hill.

Biggs, P. J., & Ling, C. C. (1979). Electrons as the cause of the observed dmax shift with field size in high energy photon beams. *Medical Physics*, *6*(4), 291–5. https://doi.org/10.1118/1.594580

Butson, M. J., Cheung, T., Yu, P., & Metcalfe, P. (2000). Effects on skin dose from unwanted air gaps under bolus in photon beam radiotherapy, *32*, 201–204.

Butson, M. J., Yu, P. K. N., & Metcalfe, P. E. (1998). Measurement of off-axis and peripheral skin dose using radiochromic film. *Physics in Medicine and Biology*, *43*(9), 2647–2650. https://doi.org/10.1088/0031-9155/43/9/015

Butson, M. J., Yu, P. K. N., & Metcalfe, P. E. (1999). Extrapolated surface dose measurements with radiochromic film. *Medical Physics*, *26*(3), 485–488. https://doi.org/10.1118/1.598539

Christ, G. (1995). White polystyrene as a substitute for water in high energy photon dosimetry. *Medical Physics*, *22*(12), 2097–2100.

Cleland, M. R., & Road, J. (1984). Proceedings of the 1984 Linear Accelerator Conference , Seeheim , Germany Proceedings of the 1984 Linear Accelerator Conference , Seeheim , Germany, (3), 496–500.

Easson, E. C., & Pointon, R. C. S. (2012). *The radiotherapy of malignant disease* (2nd ed.). Springer Science & Business Media.

Ettinger, S. J., & Feldman, E. C. (2009). *Textbook of Veterinary Internal Medicine-eBook*. Elsevier health sciences.

Ferreira, B. C., Lopes, M. C., & Capela, M. (2009). Evaluation of an Epson flatbed scanner to read Gafchromic EBT films for radiation dosimetry. *Physics in Medicine and Biology*, *54*(4), 1073–1085. https://doi.org/10.1088/0031-9155/54/4/017

Fuller, C. D., & Thomas, C. R. (2008). *Biliary tract and gallbladder cancer: diagnosis and therapy*. Demos Medical Publishing.

Gerbi, B. J., & Khan, F. M. (1990). Measurement of dose in the buildup region using fixed-separation plane-parallel ionization chambers. *Medical Physics*, *17*(1), 17–26. https://doi.org/10.1118/1.596522

Hamm, R. W. (1988). Proceedings of the 1986 International Linac Conference, Stanford,

California, USA, 33–36.

Hamm, R. W. (1990). *Commercial applications of linacs*, Robert W. Hamm AccSys Technology, Inc., 1177 Quarry Lane, Pleasanton, CA 94566.

Hillier, S. G., Kitchener, H. C., & Neilson, J. P. (1996). *Scientific essentials of reproductive medicine* (1st ed.). W. B. Saunders Co., London.

Hsu, S., Roberson, P. L., Chen, Y., Marsh, R. B., Pierce, L. J., & Moran, J. M. (2008). Assessment of skin dose for breast chest wall radiotherapy as a function of bolus material, *2593*. https://doi.org/10.1088/0031-9155/53/10/010

Ignatius, K. (2015). Assessment of the effect of beam modifiers on skin dose for external beam radiotherapy using Gafchromic EBT2 films. University of Ghana, Legon. http://ugspace.ug.edu.gh

International Atomic Energy Agency. (2000). *Absorbed Dose Determination in External Beam Radiotherapy*. *IAEA Technical Report Series No.398*. https://doi.org/10.1097/00004032-200111000-00017

International Commission on Radiation Units and Measurements. (1976). *Determination of absorbed dose in a patient irradiated by beams of X or gamma rays in radiotherapy procedures*. Bethesda, Md., U.S.A.

International Commission on Radiation Units and Measurements. (1985). *Determination of dose equivalents resulting from external radiation sources*. Bethesda, Md., U.S.A.

Johns, H. E., & Rawlinson, J. A. (1976). Desirable characteristics of high energy photons

and electrons.In: Kramer, S., Suntharalingam, N., Zinniger, G.F., eds. *High Energy Photons and Electrons*, John Wiley & Sons, New York, 11.

Jones, D. (1994). ICRU report 50—prescribing, recording and reporting photon beam therapy. *Medical Physics*, *21*(6), 833–834.

Karabedian, J. A., & Blackwelder, M. W. (1992, January 21). Polystyrene foam sheet manufacture. Google Patents.

Khan, F. M., & Gibbons, J. P. (2014). *The physics of radiation therapy* (5th ed.). Lippincott Williams & Wilkins, Philadelphia.

Khan, F. M., Moore, V. C., & Levitt, S. H. (1973). Effect of various atomic number absorbers on skin dose for 10-MeV X rays. *Radiology*, *109*(1), 209–212.

Khan, Y., Villarreal-Barajas, J. E., Udowicz, M., Sinha, R., Muhammad, W., Abbasi, A. N., & Hussain, A. (2013). Clinical and Dosimetric Implications of Air Gaps between Bolus and Skin Surface during Radiation Therapy. *Journal of Cancer Therapy*, *4*(September), 1251–1255. https://doi.org/10.4236/jct.2013.47147

Kim, S., Shin, H., Kay, C. S., & Son, S. H. (2014). A Customized Bolus Produced Using a 3-Dimensional Printer for Radiotherapy, *9*(10). https://doi.org/10.1371/journal.pone.0110746

Knapp, E. A. (1976). *Applications of linear accelerators*, E. A. Knapp University of California Los Alamos, New Mexico 87545, 115–118.

Kry, S. F., Smith, S. A., Weathers, R., & Stovall, M. (2012). Skin dose during radiotherapy: a summary and general estimation technique. *Journal of Applied*

Clinical Medical Physics, *13*(3), 20–34.

Lamb, A., & Blake, S. (1998). Investigation and modelling of the surface dose from linear accelerator produced 6 and 10 MV photon beams. *Physics in Medicine and Biology*, *43*(5), 1133–1146. https://doi.org/10.1088/0031-9155/43/5/006

Landberg, T., Chavaudra, J., Dobbs, J., Gerard, J.-P., Hanks, G., Horiot, J.-C., … Svensson, H. (1999). Report 62. *Journal of the International Commission on Radiation Units and Measurements*, *32*(1). Retrieved from http://dx.doi.org/10.1093/jicru/os32.1.Report62

Lee, N., Chuang, C., Quivey, J. M., Phillips, T. L., Akazawa, P., Verhey, L. J., & Xia, P. (2002). Skin toxicity due to intensity-modulated radiotherapy for head-and-neck carcinoma. *International Journal of Radiation Oncology Biology Physics*, *53*(3), 630–637. https://doi.org/10.1016/S0360-3016(02)02756-6

León Marroquin, E. Y., Herrera González, J. A., Camacho López, M. A., Villarreal Barajas, J. E., & García-Garduño, O. A. (2016). Evaluation of the uncertainty in an EBT3 film dosimetry system utilizing net optical density. *Journal of Applied Clinical Medical Physics*, *17*(5), 466–481. https://doi.org/10.1120/jacmp.v17i5.6262

Lewis, D. (2009). Gafchromic ® EBT2. *Ashland*, 1–17.

Marbach, J. R., & Almond, P. R. (1977). Scattered photons as the cause for the observed dmax shift with field size in high-energy photon beams. *Medical Physics*, *4*(4), 310–314.

Marinello, G., & Dutreix, A. (1973). *Etude dosimétrique d'un faisceau de rayons X de 25*

MV Dosimetric study of a 25 MV X-ray beam. *J Radiol Electrol*.

Medina, A. L., Teijeiro, A., Garcia, J., Esperon, J., Terron, J. A., Ruiz, D. P., & Carrion, M. C. (2005). Characterization of electron contamination in megavoltage photon beams. *Medical Physics*, *32*(5), 1281–1292. https://doi.org/10.1118/1.1895793

Nichiporov, D., Kostjuchenko, V., Puhl, J. M., Bensen, D. L., Desrosiers, M. F., Dick, C. E., Mclaughlin, W. L., Kojima, T., Coursey, B. M., Zink, S. (1995). Investigation of applicability of alanine and radiochromic detectors to dosimetry of proton clinical beams. *Applied Radiation and Isotopes*, *46*(12), 1355–1362. https://doi.org/10.1016/0969-8043(95)00213-W

Nilsson, B., & Brahme, A. (1986). Electron contamination from photon beam collimators. *Radiotherapy and Oncology*, *5*(3), 235–244. https://doi.org/10.1016/S0167-8140(86)80053-6

Niroomand-Rad, A., Blackwell, C. R., Coursey, B. M., Gall, K. P., Galvin, J. M., McLaughlin, W. L., Meigooni, A. S., Nath, R., Rodgers, J. E. Soares, C. G. (1998). Radiochromic film dosimetry: Recommendations of AAPM Radiation Therapy Committee Task Group 55. *Medical Physics*. https://doi.org/10.1118/1.598407

Padikal, T. N., & Deye, J. A. (1978). Electron contamination of a high-energy x-ray beam. *Physics in Medicine and Biology*, *23*(6), 1086–1092. https://doi.org/10.1088/0031-9155/23/6/004

Podgorsak, E. B. (2005). Radiation Oncology Physics : A Handbook for Teachers and Students. *IAEA*, 219–271.

Podgorsak, E. B. (2005). Treatment machines for External Beam RadioTherapy. *Radiation Oncology Physics: A Handbook for Teachers and Students. IAEA, Vienna, Austria*, 123--160.

Rajan, G., & Izewska, J. (2012). Chapter 3. Radiation Dosimeters. *Radiation Oncology Physics: A Handbook for Teachers and Students*, 657.

Rapley, P. (2006). Surface dose measurement using TLD powder extrapolation. *Medical Dosimetry*, *31*(3), 209–215. https://doi.org/10.1016/j.meddos.2006.02.003

Rawlinson, J. A., Arlen, D., & Newcombe, D. (1992). Design of parallel plate ion chambers for buildup measurements in megavoltage photon beams. *Medical Physics*, *19*(3), 641–648. https://doi.org/10.1118/1.596896

Saylor, W. L., & Quillin, R. (1971). Methods for the enhancement of skin sparing in cobalt 60 teletherapy. *Amer. J. Roentgenol.* Retrieved from http://ovidsp.ovid.com/ovidweb.cgi?T=JS&PAGE=reference&D=emcl1&NEWS=N&AN=291114187

Scalzetti, E. M., Huda, W., Bhatt, S., & Ogden, K. M. (2008). A method to obtain mean organ doses in a RANDO phantom. *Health Physics*, *95*(2), 241–244. https://doi.org/10.1097/01.HP.0000310997.09116.e3

Sroka, M., Reguła, J., & Łobodziec, W. (2010). The influence of the bolus-surface distance on the dose distribution in the build-up region. *Reports of Practical Oncology and Radiotherapy*, *15*(6), 161–164. https://doi.org/10.1016/j.rpor.2010.09.003

Stathakis, S., Li, J. S., Paskalev, K., Yang, J., Wang, L., & Ma, C. M. (2006). Ultra-thin TLDs for skin dose determination in high energy photon beams. *Physics in Medicine and Biology*, *51*(14), 3549–3567. https://doi.org/10.1088/0031-9155/51/14/018

Stevens, M. A., Turner, J. R., Hugtenburg, R. P., & Butler, P. H. (1996). High-resolution dosimetry using radiochromic film and a document scanner. *Physics in Medicine and Biology*, *41*(11), 2357–2365. https://doi.org/10.1088/0031-9155/41/11/008

The International Commission on Radiological Protection. (2007). The 2007 Recommendations of the International Commission on Radiological Protection. ICRP publication 103. *Annals of the ICRP*, *37*(2–4), 1–332. https://doi.org/10.1016/j.icrp.2007.10.003

Vatnitsky, S. M. (1997). Radiochromic film dosimetry for clinical proton beams. *Applied Radiation and Isotopes*, *48*(5), 643–651. https://doi.org/10.1016/S0969-8043(97)00342-4

Vatnitsky, S. M., Schulte, R. W. M., Galindo, R., Meinass, H. J., & Miller, D. W. (1997). Radiochromic film dosimetry for verification of dose distributions delivered with proton-beam radiosurgery. *Physics in Medicine and Biology*, *42*(10), 1887–1898. https://doi.org/10.1088/0031-9155/42/10/003

Velkley, D. E., Manson, D. J., Purdy, J. A., & Oliver, G. D. (1975). Build up region of megavoltage photon radiation sources. *Medical Physics*, *2*(1), 14–19. https://doi.org/10.1118/1.594158

Vyas, V., Palmer, L., Mudge, R., Jiang, R., Fleck, A., Schaly, B., … Charland, P. (2013).

On bolus for megavoltage photon and electron radiation therapy. *Medical Dosimetry*, *38*(3), 268–273. https://doi.org/10.1016/j.meddos.2013.02.007

Walsh, M., & Crumbie, A. (2007). *Watson's Clinical Nursing and Related Sciences E-Book* (7th ed.). Elsevier Health Sciences, Bailliere Tindall.

Yadav, G., Yadav, R. S., & Kumar, A. (2009). Skin dose estimation for various beam modifiers and source-to-surface distances for 6MV photons. *Journal of Medical Physics / Association of Medical Physicists of India*, *34*(2), 87–92. https://doi.org/10.4103/0971-6203.51935

Zhu, T. C., & Palta, J. R. (1998). Electron contamination in 8 and 18 MV photon beams. *Medical Physics*, *25*(1), 12–19. https://doi.org/10.1118/1.598169

APPENDIX

APPENDIX A

Table A. 1: Conversion of ion chamber readings to doses for 5×5 cm^2 field using 6 MV.

Roos Chamber TM 34001 S/N 002017 $N_{D,W} = 8.559\times10^7$ Gy/C $k_Q = 0.9902$ Bolus Thickness = 0.5 cm						
Distance of Bolus from Surface (cm)	Mean Ion Chamber Readings (nC)	Temperature (°C)	Pressure (kPa)	Temperature and Pressure Correction Factor	Corrected Ion Chamber Readings (nC)	Dose (Gy)
Open	4.428	25.2	100.26	1.021628	4.523E-09	0.38
0	9.420	25.1	100.26	1.021286	9.621E-09	0.82
1	9.273	25.8	100.25	1.023784	9.494E-09	0.80
2	8.773	25.8	100.26	1.023682	8.980E-09	0.76
3	8.266	26.0	100.28	1.024163	8.465E-09	0.72
4	7.767	26.0	100.28	1.024163	7.954E-09	0.67
5	7.440	26.3	100.30	1.024985	7.625E-09	0.65

Table A. 2: Conversion of ion chamber readings to doses for 10×10 cm^2 field using 6 MV.

Roos Chamber TM 34001 S/N 002017 $N_{D,W} = 8.559\times10^7$ Gy/C $k_Q = 0.9902$ Bolus Thickness = 0.5 cm						
Distance of Bolus from Surface (cm)	Mean Ion Chamber Readings (nC)	Temperature (°C)	Pressure (kPa)	Temperature and Pressure Correction Factor	Corrected Ion Chamber Readings (nC)	Dose (Gy)
Open	5.175	25.2	100.26	1.021628	5.287E-09	0.45
0	10.160	25.1	100.26	1.021286	1.038E-08	0.88
1	10.200	25.8	100.25	1.023784	1.044E-08	0.89
2	10.205	25.8	100.26	1.023682	1.045E-08	0.89
3	10.160	26.0	100.28	1.024163	1.041E-08	0.88
4	9.994	26.0	100.28	1.024163	1.023E-08	0.87
5	9.817	26.3	100.30	1.024985	1.006E-08	0.85

Table A. 3: Conversion of ion chamber readings to doses for 15×15 cm^2 field using 6 MV.

Roos Chamber TM 34001 S/N 002017 $N_{D,W} = 8.559\times10^7$ Gy/C $k_Q = 0.9902$ Bolus Thickness = 0.5 cm						
Distance of Bolus from Surface (cm)	Mean Ion Chamber Readings (nC)	Temperature (°C)	Pressure (kPa)	Temperature and Pressure Correction Factor	Corrected Ion Chamber Readings (nC)	Dose (Gy)
Open	5.868	25.2	100.26	1.021628	5.995E-09	0.51
0	10.700	25.1	100.26	1.021286	1.093E-08	0.93
1	10.750	25.8	100.25	1.023784	1.101E-08	0.93
2	10.810	25.8	100.26	1.023682	1.107E-08	0.94
3	10.860	26.0	100.28	1.024163	1.112E-08	0.94
4	10.855	26.0	100.28	1.024163	1.112E-08	0.94
5	10.820	26.3	100.30	1.024985	1.109E-08	0.94

Table A. 4: Conversion of ion chamber readings to doses for 20×20 cm^2 field using 6 MV.

Roos Chamber TM 34001 S/N 002017 $N_{D,W} = 8.559\times10^7$ Gy/C $k_Q = 0.9902$ Bolus Thickness = 0.5 cm						
Distance of Bolus from Surface (cm)	Mean Ion Chamber Readings (nC)	Temperature (°C)	Pressure (kPa)	Temperature and Pressure Correction Factor	Corrected Ion Chamber Readings (nC)	Dose (Gy)
Open	6.582	25.2	100.26	1.021628	6.724E-09	0.57
0	11.210	25.1	100.26	1.021286	1.145E-08	0.97
1	11.250	25.8	100.25	1.023784	1.152E-08	0.98
2	11.315	25.8	100.26	1.023682	1.158E-08	0.98
3	11.375	26.0	100.28	1.024163	1.165E-08	0.99
4	11.420	26.0	100.28	1.024163	1.170E-08	0.99
5	11.420	26.3	100.30	1.024985	1.171E-08	0.99

Table A. 5: Conversion of ion chamber readings to doses for 5×5 cm^2 field using 15 MV.

Roos Chamber TM 34001 S/N 002017 $N_{D,W}$ = 8.559×10^7 Gy/C k_Q = 0.9714 Bolus Thickness = 1 cm						
Distance of Bolus from Surface (cm)	Mean Ion Chamber Readings (nC)	Temperature (°C)	Pressure (kPa)	Temperature and Pressure Correction Factor	Corrected Ion Chamber Readings (nC)	Dose (Gy)
Open	2.632	25.2	100.26	1.021628	2.689E-09	0.22
0	9.335	25.1	100.26	1.021286	9.534E-09	0.79
1	8.981	25.6	100.25	1.023100	9.188E-09	0.76
2	8.180	25.9	100.26	1.024025	8.377E-09	0.70
3	7.372	26.0	100.27	1.024265	7.551E-09	0.63
4	6.702	26.2	100.30	1.024643	6.867E-09	0.57
5	6.201	26.3	100.30	1.024985	6.356E-09	0.53

Table A. 6: Conversion of ion chamber readings to doses for 10×10 cm^2 field using 15 MV.

Roos Chamber TM 34001 S/N 002017 $N_{D,W}$ = 8.559×10^7 Gy/C k_Q = 0.9714 Bolus Thickness = 1 cm						
Distance of Bolus from Surface (cm)	Mean Ion Chamber Readings (nC)	Temperature (°C)	Pressure (kPa)	Temperature and Pressure Correction Factor	Corrected Ion Chamber Readings (nC)	Dose (Gy)
Open	3.553	25.2	100.26	1.021628	3.630E-09	0.30
0	10.350	25.1	100.26	1.021286	1.057E-08	0.88
1	10.385	25.6	100.25	1.023100	1.062E-08	0.88
2	10.260	25.9	100.26	1.024025	1.051E-08	0.87
3	10.010	26.0	100.27	1.024265	1.025E-08	0.85
4	9.681	26.2	100.29	1.024745	9.920E-09	0.82
5	9.326	26.3	100.30	1.024985	9.559E-09	0.79

Table A. 7: Conversion of ion chamber readings to doses for 15×15 cm^2 field using 15 MV.

Roos Chamber TM 34001 S/N 002017 $N_{D,W}$ = 8.559×10^7 Gy/C k_Q = 0.9714 Bolus Thickness = 1 cm						
Distance of Bolus from Surface (cm)	Mean Ion Chamber Readings (nC)	Temperature (°C)	Pressure (kPa)	Temperature and Pressure Correction Factor	Corrected Ion Chamber Readings (nC)	Dose (Gy)
Open	4.451	25.2	100.26	1.021628	4.547E-09	0.38
0	11.080	25.1	100.26	1.021286	1.132E-08	0.94
1	11.145	25.6	100.25	1.023100	1.140E-08	0.95
2	11.110	25.9	100.26	1.024025	1.138E-08	0.95
3	11.060	26.0	100.28	1.024163	1.133E-08	0.94
4	10.960	26.2	100.29	1.024745	1.123E-08	0.93
5	10.820	26.3	100.30	1.024985	1.109E-08	0.92

Table A. 8: Conversion of ion chamber readings to doses for 20×20 cm^2 field using 15 MV.

Roos Chamber TM 34001 S/N 002017 $N_{D,W}$ = 8.559×10^7 Gy/C k_Q = 0.9714 Bolus Thickness = 1 cm						
Distance of Bolus from Surface (cm)	Mean Ion Chamber Readings (nC)	Temperature (°C)	Pressure (kPa)	Temperature and Pressure Correction Factor	Corrected Ion Chamber Readings (nC)	Dose (Gy)
Open	5.378	25.2	100.26	1.021628	5.494E-09	0.46
0	11.703	25.1	100.26	1.021286	1.195E-08	0.99
1	11.780	25.6	100.25	1.023100	1.205E-08	1.00
2	11.765	25.9	100.26	1.024025	1.205E-08	1.00
3	11.770	26.0	100.28	1.024163	1.205E-08	1.00
4	11.735	26.2	100.29	1.024745	1.203E-08	1.00
5	11.695	26.3	100.30	1.024985	1.199E-08	1.00

APPENDIX B

Table B. 1: Mean pixel values of blue, green and red channels for GafChromic EBT3 film calibration using 6 MV.

Prescribed dose (Gy)	Mean Pixel Values		
	Blue Channel	Green Channel	Red Channel
0.0	71.317	122.290	85.199
0.2	69.722	114.190	77.067
0.4	69.507	110.651	71.345
0.8	68.278	103.530	64.628
1.6	65.817	92.094	55.882
2.4	63.059	81.839	49.768
3.2	61.351	74.732	46.832
4.0	58.900	67.902	43.478
5.0	57.177	62.120	41.920

Table B. 2: Mean pixel values of blue, green and red channels for GafChromic EBT3 film calibration using 15 MV.

Prescribed dose (Gy)	Mean Pixel Values		
	Blue Channel	Green Channel	Red Channel
0.0	72.710	123.877	86.720
0.2	70.458	116.756	76.432
0.4	70.118	112.873	72.670
0.8	68.140	103.490	63.443
1.6	66.172	92.754	54.987
2.4	64.017	83.873	49.519
3.2	61.561	75.499	46.151
4.0	59.140	68.839	43.266
5.0	57.422	63.124	41.520

Table B. 3: Percentage error between prescribed dose and measured dose for the red channel calibration curve using 6 MV.

Prescribed Dose (Gy)	Measured Dose (Gy)	Percentage Error (%)
0.0	0.0	0.00
0.2	0.2	21.21
0.4	0.4	4.12
0.8	0.8	4.23
1.6	1.6	1.47
2.4	2.4	1.32
3.2	3.1	3.66
4.0	4.2	4.71
5.0	4.9	2.05
	Mean Percentage Error:	1.75

Table B. 4: Percentage error between prescribed dose and measured dose for the red channel calibration curve using 15 MV.

Prescribed Dose (Gy)	Measured Dose (Gy)	Percentage Error (%)
0.0	0.0	0.00
0.2	0.2	12.72
0.4	0.3	22.05
0.8	0.8	2.31
1.6	1.5	8.72
2.4	2.2	7.04
3.2	3.0	6.39
4.0	4.0	1.10
5.0	4.7	5.25
	Mean Percentage Error:	7.29

APPENDIX C

Table C. 1: Mean pixel values and optical densities of Gafchromic films used for measuring surface doses for 6 MV photon beam using a field size of 5×5 cm^2.

Distance of Bolus from Surface (cm)	Mean Pixel Value	Optical Density
Open	70.890	0.075
0	63.841	0.121
1	64.227	0.118
2	65.220	0.111
3	65.134	0.110
4	66.102	0.102
5	66.227	0.102

Table C. 2: Mean pixel values and optical densities of Gafchromic films used for measuring surface doses for 6 MV photon beam using a field size of 10×10 cm^2.

Distance of Bolus from Surface (cm)	Mean Pixel Value	Optical Density
Open	69.201	0.080
0	62.527	0.125
1	62.709	0.125
2	62.682	0.125
3	62.721	0.123
4	62.739	0.123
5	63.031	0.120

Table C. 3: Mean pixel values and optical densities of Gafchromic films used for measuring surface doses for 6 MV photon beam using a field size of 15×15 cm^2.

Distance of Bolus from Surface (cm)	Mean Pixel Value	Optical Density
Open	68.363	0.086
0	61.966	0.127
1	61.767	0.128
2	61.154	0.132
3	61.489	0.132
4	61.706	0.130
5	61.240	0.133

Table C. 4: Mean pixel values and optical densities of Gafchromic films used for measuring surface doses for 6 MV photon beam using a field size of 20×20 cm^2.

Distance of Bolus from Surface (cm)	Mean Pixel Value	Optical Density
Open	67.258	0.094
0	61.267	0.134
1	61.236	0.135
2	61.444	0.133
3	61.683	0.132
4	61.301	0.135
5	61.603	0.132

Table C. 5: Mean pixel values and optical densities of Gafchromic films used for measuring surface doses for 15 MV photon beam using a field size of 5×5 cm^2.

Distance of Bolus from Surface (cm)	Mean Pixel Value	Optical Density
Open	73.042	0.063
0	60.757	0.140
1	61.911	0.133
2	62.398	0.128
3	63.779	0.119
4	64.560	0.112
5	66.511	0.104

Table C. 6: Mean pixel values and optical densities of Gafchromic films used for measuring surface doses for 15 MV photon beam using a field size of 10×10 cm^2.

Distance of Bolus from Surface (cm)	Mean Pixel Value	Optical Density
Open	70.170	0.072
0	58.987	0.149
1	59.322	0.147
2	59.424	0.146
3	59.908	0.142
4	60.147	0.140
5	61.376	0.134

Table C. 7: Mean pixel values and optical densities of Gafchromic films used for measuring surface doses for 15 MV photon beam using a field size of 15×15 cm^2.

Distance of Bolus from Surface (cm)	Mean Pixel Value	Optical Density
Open	68.230	0.086
0	58.637	0.151
1	58.313	0.154
2	58.566	0.154
3	58.729	0.152
4	58.859	0.151
5	58.986	0.148

Table C. 8: Mean pixel values and optical densities of Gafchromic films used for measuring surface doses for 20 MV photon beam using a field size of 20×20 cm^2.

Distance of Bolus from Surface (cm)	Mean Pixel Value	Optical Density
Open	66.958	0.096
0	57.967	0.159
1	58.076	0.157
2	57.958	0.159
3	57.397	0.162
4	57.468	0.161
5	57.279	0.164

APPENDIX D

Table D. 1: Percentage error between surface doses measured using ion chambers and GafChromic films for 6 MV photon beams with field size of 5×5 cm^2.

Distance of Bolus from Surface (cm)	Surface Dose using Ion Chamber (Gy)	Surface Dose using GafChromic film (Gy)	Percentage Error (%)
Open	0.38	0.40	4.16
0	0.82	0.84	3.15
1	0.80	0.82	1.44
2	0.76	0.74	2.18
3	0.72	0.73	2.02
4	0.67	0.66	2.77
5	0.65	0.65	0.32

Table D. 2: Percentage error between surface doses measured using ion chambers and GafChromic films for 6 MV photon beams with field size of 10×10 cm^2.

Distance of Bolus from Surface (cm)	Surface Dose using Ion Chamber (Gy)	Surface Dose using GafChromic film (Gy)	Percentage Error (%)
Open	0.45	0.44	0.72
0	0.88	0.89	0.64
1	0.89	0.88	0.14
2	0.89	0.89	0.16
3	0.88	0.87	1.77
4	0.87	0.86	0.81
5	0.85	0.84	1.79

Table D. 3: Percentage error between surface doses measured using ion chambers and GafChromic films for 6 MV photon beams with field size of 15×15 cm^2.

Distance of Bolus from Surface (cm)	Surface Dose using Ion Chamber (Gy)	Surface Dose using GafChromic film (Gy)	Percentage Error (%)
Open	0.51	0.50	2.52
0	0.93	0.91	2.11
1	0.93	0.92	1.60
2	0.94	0.96	2.57
3	0.94	0.96	2.20
4	0.94	0.94	0.20
5	0.94	0.97	3.53

Table D. 4: Percentage error between surface doses measured using ion chambers and GafChromic films for 6 MV photon beams with field size of 20×20 cm^2.

Distance of Bolus from Surface (cm)	Surface Dose using Ion Chamber (Gy)	Surface Dose using GafChromic film (Gy)	Percentage Error (%)
Open	0.57	0.58	1.04
0	0.97	0.99	1.64
1	0.98	0.99	1.55
2	0.98	0.97	0.80
3	0.99	0.96	2.90
4	0.99	0.99	0.21
5	0.99	0.96	3.16

Table D. 5: Percentage error between surface doses measured using ion chambers and GafChromic films for 15 MV photon beams with field size of 5×5 cm^2.

Distance of Bolus from Surface (cm)	Surface Dose using Ion Chamber (Gy)	Surface Dose using GafChromic film (Gy)	Percentage Error (%)
Open	0.22	0.22	0.05
0	0.79	0.82	3.47
1	0.76	0.75	1.44
2	0.70	0.71	2.07
3	0.63	0.63	0.62
4	0.57	0.58	1.48
5	0.53	0.52	2.52

Table D. 6: Percentage error between surface doses measured using ion chambers and GafChromic films for 15 MV photon beams with field size of 10×10 cm^2.

Distance of Bolus from Surface (cm)	Surface Dose using Ion Chamber (Gy)	Surface Dose using GafChromic film (Gy)	Percentage Error (%)
Open	0.30	0.28	6.56
0	0.88	0.91	3.42
1	0.88	0.88	0.11
2	0.87	0.88	0.17
3	0.85	0.84	1.50
4	0.82	0.82	0.50
5	0.79	0.76	3.77

Table D. 7: Percentage error between surface doses measured using ion chambers and GafChromic films for 15 MV photon beams with field size of 15×15 cm^2.

Distance of Bolus from Surface (cm)	Surface Dose using Ion Chamber (Gy)	Surface Dose using GafChromic film (Gy)	Percentage Error (%)
Open	0.38	0.38	0.55
0	0.94	0.93	1.20
1	0.95	0.96	0.99
2	0.95	0.95	0.44
3	0.94	0.94	0.42
4	0.93	0.93	0.52
5	0.92	0.90	2.80

Table D. 8: Percentage error between surface doses measured using ion chambers and GafChromic films for 15 MV photon beams with field size of 20×20 cm^2.

Distance of Bolus from Surface (cm)	Surface Dose using Ion Chamber (Gy)	Surface Dose using GafChromic film (Gy)	Percentage Error (%)
Open	0.46	0.45	1.17
0	0.99	1.01	1.24
1	1.00	0.99	1.55
2	1.00	1.01	0.47
3	1.00	1.03	3.24
4	1.00	1.02	2.08
5	1.00	1.06	5.89